ENERGY AND ANGULAR MOMENTUM TRANSFER WITH CIRCULAR RYDBERG STATES

A THESIS SUBMITTED TO
THE GRADUATE SCHOOL OF ENGINEERING AND SCIENCE
OF BILKENT UNIVERSITY
IN PARTIAL FULFILLMENT OF THE REQUIREMENTS FOR
THE DEGREE OF
MASTER OF SCIENCE
IN
PHYSICS

By
Mohammad Mujaheed Aliyu
August 2017

Energy and angular momentum transfer with circular Rydberg states
By Mohammad Mujaheed Aliyu
August 2017

We certify that we have read this thesis and that in our opinion it is fully adequate, in scope and in quality, as a thesis for the degree of Master of Science.

Sebastian Wüster(Advisor)

Mehmet Özgür Oktel

Mehmet Emre Tasgin

Approved for the Graduate School of Engineering and Science:

Ezhan Karaşan
Director of the Graduate School

ABSTRACT

ENERGY AND ANGULAR MOMENTUM TRANSFER WITH CIRCULAR RYDBERG STATES

Mohammad Mujaheed Aliyu
M.S. in Physics
Advisor: Sebastian Wüster
August 2017

Circular states belong to a class of Rydberg states having maximum angular momentum. These states, compared to other Rydberg states, have longer lifetimes, and in the classical limit resemble circular Bohr-like orbits. The long lifetime makes them suitable for use in cavity-QED experiments, precision measurements and simulation of quantum energy transport in biological systems.

Energy transfer has earlier been studied using non-circular Rydberg states. Here, we look at interacting ultra-cold atoms in circular Rydberg states, and show how energy and angular momentum transfer can be studied in much larger systems due to improved lifetimes. As we show this is made possible by reducing the number of interacting two-atom states involved in transport to just two, via dipole-dipole selection rules. We determine the trapping precision required to maintain this simple description. Finally we present initial investigations to what extent transport with circular states can be modelled classically.

Our results indicate that circular Rydberg states can be used for quantum simulations of energy and angular momentum transport for longer times than low-lying angular momentum states. Through using a pair of circular states with comparable C_3 values Rydberg atomic chains could also find application in quantum information transfer mechanisms.

Keywords: Key one, key two.

ÖZET

DAIRESEL RYDBERG DALGA DURUMLARI ILE ENERJI VE AÇISAL MOMENTUM TRANSFERI

Mohammad Mujaheed Aliyu
Fizik, Yüksek Lisans
Tez Danışmanı: Sebastian Wüster
August 21, 2017

Dairesel dalga durumları, Rydberg dalga durumlarından açısal momentumu en yüksek olandır. Bu dalga durumları diğer Rydberg dalga durumları ile kıyasladığında daha uzun ömürlüdür ve klasik limitte çembersel Bohr-gibi yörünlere benzeşirler. Uzun ömürleri bu dalga durumlarının kobuk kuvantum elektrodinamii deneylerinde, hassas ölçümlerde ve biyolojik sistemlerdeki kuantum enerji transferin simülasyonlarında kullanışlı olmalarını salar.

Enerji transferi daha öncesinde dairesel olmayan Rydberg dalga durumlarında çalışıldı. Burada biz, dairesel enerji dalga durumlarındaki ultrasoğuk etkileşim halindeki atomları inceledik ve artırılmış ömürlerinden ötürü daha büyük sistemlerde enerji ve açısal momentum transferinin çalışılabileceini gösterdik. Gösterdiğimiz gibi, etkileşime giren iki atomlu transfere katılan dalga durumlarını, dipol-dipol Rydberg seçim kurallarını kullanarak sadece ikiye indirmeyi başardık. Bu basit tarifi geçerli kılmak için hapsetme hassasiyetini belirledik. Son olarak, dairesel durumlarda hangi sınıra kadar iletimin klasik olarak modellenebileceğini soruşturduk.

Aldığımız sonuçlar, çembersel Rydberg durumlarının enerji ve açısal momentum aktarımı simülasyonlarında düşük açısal momentumlu durumlara kıyasla daha uzun süre kullanılabileceğini gösterdi. Bir çift benzer C_3 değerine sahip çembersel durumlar kullanılarak oluşturulan Rydberg atomları zinciri, kuantum bilgi aktarımı mekanizmalarında da kullanılabilir.

Anahtar sözcükler: Anahtar Sözlerim.

Acknowledgement

I would like to express my deepest gratitude to my supervisor, Prof Sebastian Wüster, for agreeing to take me into his group, and his generous guidance and understanding in my moments of madness during this study.

My deep gratitude also to Prof Ahmet Gökalp for making me understand that the discipline to use proper concepts in attacking quantum mechanical problems plays just as crucial a role as the intuition one has for the subject. The complaints and occasional arguments other students and I usually had with him in his office regarding exam grades remain one of the clearest memories of my stay here.

To Prof Ceyhun Bulutay I say thank you, for all the advice and guidance, none more clear in my mind than the one that led me to this group and this thesis, thank you.

I would also like to thank the few friends I made during my stay here, few yet many in many ways. It has been two good years because you were good, thank you.

And finally my family, what can I say?, 'I'm everything I am because of you', thank you.

Declaration

This thesis is the result of research done between August 2016 and August 2017 at the Department of physics, Faculty of sciences, Bilkent University, Ankara, Turkey.

I worked jointly with Alptuğ Ulugöl on the quantum-classical comparison in chapter 2. The classical calculations were performed by Alptuğ, and the quantum mechanical ones by myself.

The code for calculations of Rydberg-Rydberg interactions was written by my supervisor, Dr. Sebastian Wüster, and adapted by myself to suit our numerical requirements.

Contents

List of Figures

List of Tables

Chapter 1

Introduction to Ryberg Atoms and Circular Rydberg States

Rydberg states are highly excited eigenstates of an atom. They are states having high principal quantum number n, and atoms with electron(s) in these states are called Rydberg atoms. These atoms have been found to exhibit extraordinary properties [1], such as high sensitivity to external fields with n^7 scaling, large valence electron radii that scale as n^2, enhanced dipole matrix elements between states with n^2, huge van-der-Waals interaction $\frac{C_6}{R^6}$ with C_6 scaling as n^{11} and long lifetimes that scale as n^3.

Rydberg atoms had earlier been produced through techniques such as electron impact and charge excitation [2, 3], but the invention of lasers [4] made it possible to produce them at ultra-cold temperatures. It is at this low temperatures that the true exotic nature of Rydberg atoms become evident. Effects such as classical motion due to their strong van-der-Waals interactions [5], anti-blockade [6, 7], and blockade effects [8, 9] have so far been shown and even found applications in the fields of quantum optics [10] and quantum information [11].

Rydberg atoms have also been proposed to aid the field of bio-chemical

physics through quantum simulations of energy transport in photosynthetic light-harvesting complexes. This energy transfer mechanism plays a central role in this particular study.

A special class of Rydberg states called **circular Rydberg states**, corresponding to those states having maximal angular momentum ($l = n - 1, m = l$) [12], have even more exaggerated properties like longer lifetimes that scale as n^5 [13]. Their longer lifetimes make them better candidates for use in precision measurements [14, 15], cavity-QED experiments for atom-cavity coupling due to their near-perfect two-level atom-like features [16, 17, 18], and quantum information [13]. Since these states can be created only through sequential state changes involving a whole range of quantum states, special excitation techniques had to be devised in order to successfully populate them. Many such techniques for hot and cold circular state atoms have so far been proposed and realized [19, 20, 21].

Energy, angular momentum and entanglement transport [22, 23, 24] have been studied using $|ns\rangle$ and $|np\rangle$ Rydberg states. Here, we perform a theoretical study of energy and angular momentum transfer using circular Rydberg states, with the aim of inferring parameters for which transport with these states would last longer than with the $|ns\rangle$ and $|np\rangle$ states used in previous studies.

1.1 Thesis outline

In chapter 2, we review Bohr and Sommefeld's atomic model while also studying two highly excited interacting Alkali atoms in Bohr-like orbits with an eye towards formulating a classical analogue for circular Rydberg states by solving their classical Newton equations.

In chapter 3, we present a fully quantum mechanical treatment for Rydberg atoms and their interactions. We start by presenting the Hydrogen atom and show how it can be extended to Alkali atoms. Interactions between Alkali atoms follow, after which a qualitative three-level atom example is given.

Energy and angular momentum transfer using circular states is then presented, with parameters such as C_3 and C_6 also given. A more realistic case that takes into account atomic position uncertainties within their trapping regions is presented with the resulting transfer to undesirable states analysed. Analytical results for circular states are then given.

Chapter 4 deals with comparison of results from the three models used in this study.

And finally, in chapter 5 we conclude on the important results of this study and possible applications in future projects.

Chapter 2

Classical Analogue of Circular Rydberg States

The huge size of Rydberg atoms makes them good candidates to use in the study of regimes where classical and quantum mechanics produce consistent results. Here, we look at a classical picture describing a system of two interacting Rydberg atoms in states with the same energy but different angular momenta. We will study how angular momentum transfer occurs using these states. Bohr's atomic model is briefly discussed as is the Sommerfeld model, and finally angular momentum transfer between highly excited atoms using the Bohr-Sommerfeld model is studied.

2.1 Bohr's Model

The Danish physicist, Niels Bohr, in a series of papers in 1913 built on the works of Ernest Rutherford, a New Zealand-born British Nuclear physicist, to introduce a model for one-electron atoms. Bohr describes the atom as a system consisting of an electron orbiting a massive nucleus through attractive electrostatic interaction. He made certain assumptions while making his model [25], some of which are:

- The electron's motion occurs in circular orbits around the nucleus.
- The electron's angular momentum is quantized. Here, he asserted that the electron does not emit light if and only if the circumference of its orbit is an integer multiple of the Broglie wavelength.
- The motion is driven by an attractive centripetal force between the electron and the nucleus.

Using the above assumptions, starting from the second one, the following expressions were derived

$$\begin{aligned} 2\pi r &= n\lambda, \\ 2\pi r &= n\frac{h}{p}, \\ r &= n\frac{\hbar}{m_e v}, \\ m_e v r &= n\hbar. \end{aligned}$$

Where r is the orbit radius, $\hbar$ is the reduced Planck's constant, m_e is the mass of electron, v is the velocity of electron and n is a positive integer designating the atomic level. With these we have

$$L = n\hbar, \tag{2.1}$$

as the angular momentum quantization.

Considering the electrostatic attraction and centrifugal force between the nucleus and the electron, one can show that:

- The atomic radius scales as n^2,
- the electron's orbital speed scales as n^{-1},
- and the atomic energy scales as n^{-2},

like the quantum mechanical results.

This puts the electron in circular orbits around the nucleus.

The Broglie wavelength for the states we consider here,

$$\lambda_n = \frac{2\pi\hbar}{p} = \frac{2\pi\hbar}{mv_n} \tag{2.2}$$

scales as n, so that the ratio

$$\frac{\lambda_n}{2\pi r_n} = \frac{\hbar}{mv_n r_n}, \tag{2.3}$$

scales as n^{-1}. This ratio is much smaller than 1 for large values of n. We will see later in this thesis, that properties of some high n Rydberg states can be well understood from classical methods, which is a consequence of the de-Broglie wavelength being small on the scale of the orbital radius as just shown.

However, despite the successes of this model in areas such as atomic spectroscopy, several deficiencies such as: failure to predict shells and sub-shells to completely specify and distinguish atomic states, inability to explain the process of atomic 'jump' between levels and the radiation created by the accelerating electron, wrongly predicting the angular momentum of Hydrogen's ground state, and many others, held it back. To correct some of the issues associated with Bohr's model, Sommerfeld proposed the modifications discussed next.

2.2 Sommerfeld's Model

Arnold Sommerfeld's model introduces a number of changes to Bohr's which help correct some of the issues mentioned earlier. In his papers [26],[27] the following were introduced:

- Elliptic orbits: these help introduce the concept of shells and sub-shells needed to fully specify an atom's state and its place in the periodic table.
- Center of mass motion: The electron and nucleus possess a common motion, this results in the mass-dependence of the Rydberg constant, which enables

the distinction of various atomic isotopes through their emission frequency as a result of difference in the nuclear mass.

- Relativistic mass effect: This help provide an answer to the experimentally observed non-linear nature of Hydrogen's energy spectrum by adding more corrections to Bohr's calculated energies.

For the quantization he considered both radial and angular quantizations.

$$\oint p_k \, dq_k = n_k h. \tag{2.4}$$

Where p_k is the generalized momentum corresponding to the generalized coordinate q_k. With this quantization, the motion of the electron is quantized for all degrees of freedom and this led to allowed elliptic orbits.

If the polar coordinate system is adopted, the quantization goes as:

$$\oint p_r \, dr = n_r h, \tag{2.5}$$

where p_r is the radial momentum, r is the radial coordinate and n_r is an integer.

$$\oint p_\theta \, d\theta = p_\theta \oint d\theta = 2\pi p_\theta = n_\theta h, \tag{2.6}$$

where p_θ is the angular momentum, θ is the angular coordinate and n_θ is an integer. Then, if we relabel p_θ, L and n_θ as l we get:

$$L = l\hbar, \tag{2.7}$$

which is consistent with Bohr's model. This quantizations led to the following for elliptical orbits

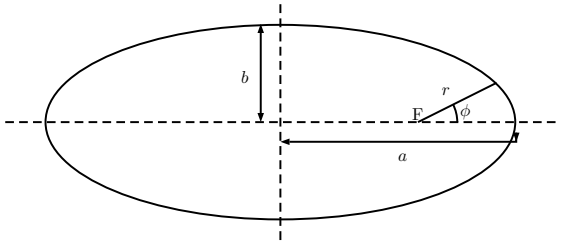

Figure 2.1: Elliptic Orbit

The semimajor axis, i.e. a, of the ellipse is given by:

$$a_n = \frac{4\pi\epsilon_0\hbar^2}{\mu e^2}\, n^2, \qquad (n = 1, 2, 3, \cdots) \tag{2.8}$$

And semiminor axis, b, by:

$$b_{nl} = \frac{4\pi\epsilon_0\hbar^2}{\mu e^2}\, ln, \qquad (l = 1, 2, \cdots, n-1) \tag{2.9}$$

where $\mu = \frac{m_e m_n}{m_e + m_n}$, is the reduced mass of electron and nucleus.

By applying Kepler's solution to a particle with fixed energy in an elliptic orbit, one can show that the energy scales as n^{-2} just like the quantum mechanical result.

However, due to experimental results' disagreement with equation 2.7, it was changed to

$$L = \sqrt{l(l+1)}\,\hbar. \tag{2.10}$$

This leads to

$$b_{nl} = \frac{4\pi\epsilon_0\hbar^2}{\mu e^2}\, \sqrt{l(l+1)}n, \quad (l = 1, 2, \cdots, n-1) \tag{2.11}$$

2.3 The circular states

As mentioned earlier, these correspond to elliptical orbits with zero eccentricity. To see this consider the equation describing an ellipse

$$\frac{x^2}{a^2} + \frac{y^2}{b^2} = 1, \tag{2.12}$$

with eccentricity

$$\sqrt{1 - \frac{b^2}{a^2}} = 0 \rightarrow b = a. \tag{2.13}$$

This means the orbits are now circular, guided by the equation

$$\frac{x^2}{r^2} + \frac{y^2}{r^2} = 1, \tag{2.14}$$

with radius r.

An atom in a circular state, therefore, is akin to one in a Bohr-like orbit guided by the modified Bohr-Sommerfeld model.

In the remainder of this chapter, we consider two atoms in circular Rydberg states having same energy but different angular momenta and study their angular momentum transfer classically. To do this, we write the coupled Newton's equations of motion guiding each atom's electron from which we numerically obtain their position at any instant in time.

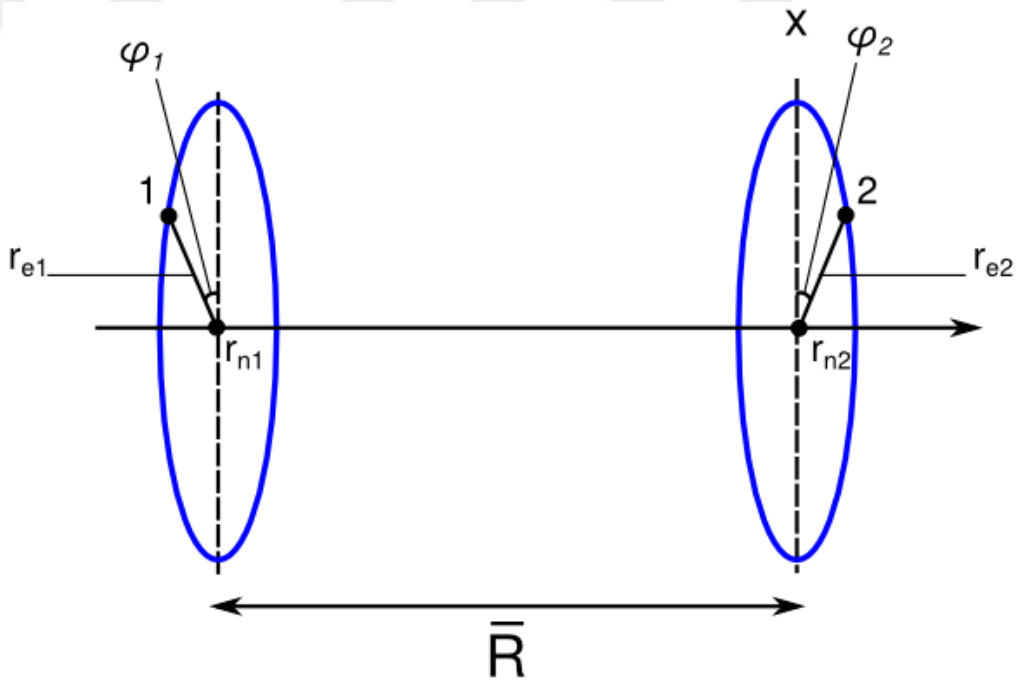

Figure 2.2: The $3D$ sketch illustrates two circular orbits lying in the x-y plane, with an offset along z between the two.

Consider a system consisting of two atoms, figure 2.2, one with nucleus at position $\mathbf{r}_{n1}$ and an electron orbiting the nucleus at $\mathbf{r}_{e1}$, and the other at $\mathbf{r}_{n2}$ with electron at $\mathbf{r}_{e2}$ so that $|\mathbf{R}| = |\mathbf{r}_{n2} - \mathbf{r}_{n1}|$.

The electrostatic force experienced by each electron can be written as

$$\vec{F}_{e1} = -\frac{e^2}{4\pi\epsilon_0}\left(\frac{\vec{r}_{e1}-\vec{r}_{n1}}{||\vec{r}_{e1}-\vec{r}_{n1}||^3} + \frac{\vec{r}_{e1}-\vec{r}_{n2}}{||\vec{r}_{e1}-\vec{r}_{n2}||^3} - \frac{\vec{r}_{e1}-\vec{r}_{e2}}{||\vec{r}_{e1}-\vec{r}_{e2}||^3}\right), \tag{2.15}$$

$$\vec{F}_{e2} = -\frac{e^2}{4\pi\epsilon_0}\left(\frac{\vec{r}_{e2}-\vec{r}_{n1}}{||\vec{r}_{e2}-\vec{r}_{n1}||^3} + \frac{\vec{r}_{e2}-\vec{r}_{n2}}{||\vec{r}_{e2}-\vec{r}_{n2}||^3} - \frac{\vec{r}_{e2}-\vec{r}_{e1}}{||\vec{r}_{e2}-\vec{r}_{e1}||^3}\right), \tag{2.16}$$

and since $\vec{F} = m_e\vec{a} = m_e\frac{d^2r}{dt^2}$, one gets

$$\frac{d^2\vec{r}_{e1}}{dt^2} = -\frac{e^2}{4\pi\epsilon_0 m_e}\left(\frac{\vec{r}_{e1}-\vec{r}_{n1}}{||\vec{r}_{e1}-\vec{r}_{n1}||^3} + \frac{\vec{r}_{e1}-\vec{r}_{n2}}{||\vec{r}_{e1}-\vec{r}_{n2}||^3} - \frac{\vec{r}_{e1}-\vec{r}_{e2}}{||\vec{r}_{e1}-\vec{r}_{e2}||^3}\right), \tag{2.17}$$

$$\frac{d^2\vec{r}_{e2}}{dt^2} = -\frac{e^2}{4\pi\epsilon_0 m_e}\left(\frac{\vec{r}_{e2}-\vec{r}_{n1}}{||\vec{r}_{e2}-\vec{r}_{n1}||^3} + \frac{\vec{r}_{e2}-\vec{r}_{n2}}{||\vec{r}_{e2}-\vec{r}_{n2}||^3} - \frac{\vec{r}_{e2}-\vec{r}_{e1}}{||\vec{r}_{e2}-\vec{r}_{e1}||^3}\right), \tag{2.18}$$

where $\vec{r}_{ei}$ is the position of i^{th} electron, $\vec{r}_{ni}$ is the position of i^{th} nucleus.

Finding r_{e1} and r_{e2} allow us to write,

$$L_1 = m_e v_{e1} r_{e1}(t) \tag{2.19}$$

$$L_2 = m_e v_{e2} r_{e2}(t) \tag{2.20}$$

as the angular momenta at any time.

For the numerical simulations we chose the nuclei to lie on the z-axis while the orbits, determined by n and l, rotate in the x-y plane with the electronic

orbital phase angles randomly defined through ϕ_1 and ϕ_2, see figure 2.2. We thus randomly pick a position on the orbits and determine the initial velocity using fixed angular momentum. Simulations are finally repeated many times to average over random initial phases ϕ_1 and ϕ_2.

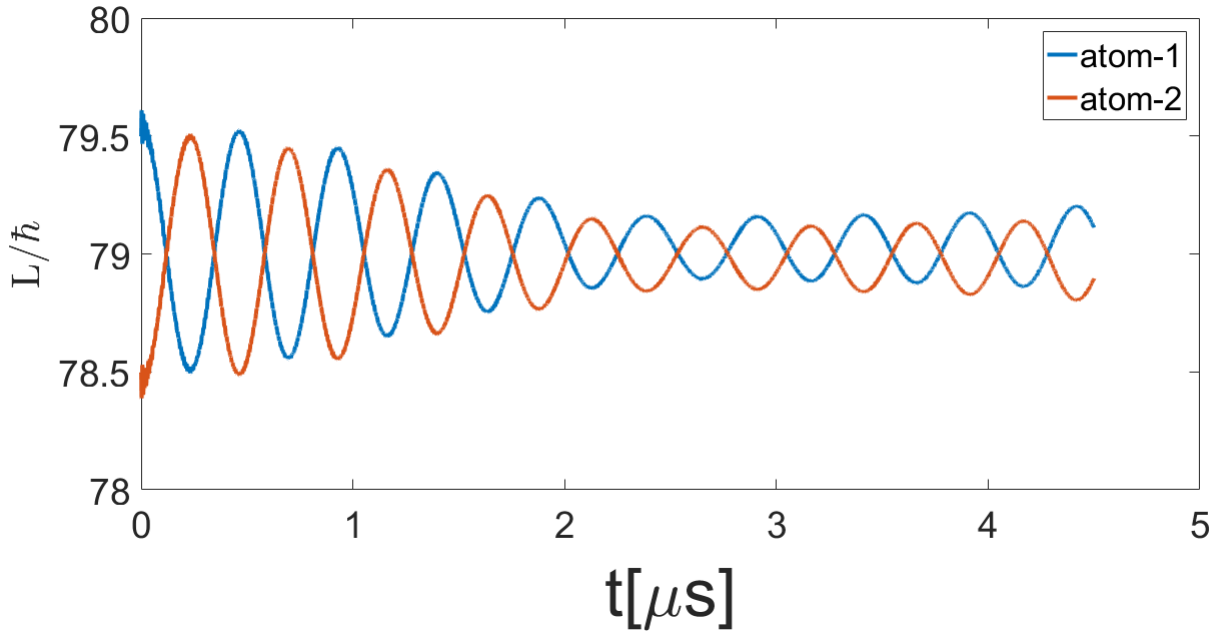

Figure 2.3: Classical result of angular momentum transfer using circular Rydberg atoms separated by R=10μm in $|n, l\rangle \rightarrow |80, 79\rangle$ and $|80, 78\rangle$. **Simulation data courtesy of Alptuğ Ulugöl.**

From the plots, the $|\mathbf{L}|$ transfer starts resonantly and lasts for $0 < t < 1\mu s$ before de-phasing sets in to damp its magnitude and oscillatory nature.

The transfer, for t $> 1\mu s$, then moves towards reaching a stable state, which, though not seen here, for t $\gg 5\mu s$ happens at $L/\hbar = 79$.

We will return to these results near the end of the thesis, where we compare them with corresponding quantum mechanical calculations.

2.4 Conclusion

We have briefly reviewed Bohr's model of the atom and pointed out its shortcomings while also introducing Sommerfeld's model that helped correct some of the issues. We then associated the trajectory of an highly excited electron of an Alkali atom to that of an ellipse, as given in the Sommerfeld model, having "zero" eccentricity, which becomes the classical analogue of "circular Rydberg states ".

We have found that the transfer is only resonant for a short time after which de-phasing sets in to damp its magnitude and oscillatory behaviour.

Chapter 3

Atoms in Circular Rydberg States and their Quantum Mechanical Interactions

In the previous chapter we saw a classical example of Rydberg-Rydberg interactions, here we present a fully quantum mechanical treatment.

Since the work presented here is on Rubidium, an alkali atom, and a good approximation for alkali atoms in Rydberg states is the Hydrogen atom, the eigenstates and eigenenergies of which can be calculated analytically, it is therefore important that we start this chapter with a brief treatment on it. Its wavefunctions will later enable us to look at analytical results.

We will then present a more accurate treatment for alkali atoms, here an effective potential $U_{eff}(r)$ will be needed due to the presence of the other electrons close to the nucleus, only numerical calculations are possible. Using numerical results, the scaling with n of some of the quantities mentioned above for circular states will be investigated, and the angular momentum transfer with circular Rydberg states presented.

Finally, we present a fully analytical calculation of the angular momentum transfer.

Note: atomic units are used throughout this chapter.

3.1 From Hydrogen to Alkali atoms

The Hydrogen atom consists of a positively charged nucleus and a single negatively charged electron in an orbit around the nucleus, interacting through the Coulomb potential

$$U_c(r) = -\frac{1}{r}. \tag{3.1}$$

The task here then is to solve the eigenvalue problem

$$H\psi(r,\theta,\phi) = E\psi(r,\theta,\phi), \tag{3.2}$$

where H is the total Hamiltonian, $\psi(r,\theta,\phi)$ the Eigenfunctions and E the Eigenenergies corresponding to the Eigenfunctions.
Specifically:

$$\psi(r,\theta,\phi) = R_{nl}(r)Y_m^l(\theta,\phi). \tag{3.3}$$

By defining

$$g_{nl}(r) = rR_{nl}(r), \tag{3.4}$$

and using spherical coordinates and some substitutions one arrives at, for the radial part, the Schrödinger equation

$$\left(-\frac{1}{2}\partial_r^2 - \frac{1}{r} + \frac{l(l+1)}{2r^2}\right) g_{nl}(r) = E_n g_{nl}(r), \tag{3.5}$$

for the Hydrogen atom, the solutions of which are available in almost all quantum mechanics books and are given by [28]:

$$R_{nl}(r) = \sqrt{\Big(\frac{2}{n}\Big)^3 \frac{(n-l-1)!}{2n(n+l)!}} \exp\Big(-\frac{\rho}{2}\Big) L^{2l+1}_{n-l-1}(\rho)\rho^l, \tag{3.6}$$

$$Y^{(l)}_{(m)}(\theta,\phi) = \sqrt{\frac{(2l+1)(l-m)!}{4\pi(l+m)!}} P^{(l)}_{(m)}(\cos\theta)\exp(im\phi), \tag{3.7}$$

where $\rho = \frac{2r}{n}$, and $L^{2l+1}_{n-l-1}(\rho)$ are generalized Laguerre polynomials and $P^{(l)}_{(m)}(\cos(\theta))$ Legendre polynomials. The eigenenergies are given by

$$E_n = -\frac{1}{2n^2}. \tag{3.8}$$

The effect of spin-orbit coupling and other corrections to the energies are not included here, nor is their effect on the radial wavefunction. This is more clearly understood when we treat the Alkali atom case.

In the case of Alkali atoms like Rubidium, the presence of non-valence electrons necessitates a change in the form of the used potential when the valence electron is not reasonably far away from the nucleus. In other words, the overlap between the Rydberg electron's wavefunctions and that of the core electrons becomes non-negligible when it isn't far away from the nucleus, hence the need for a modified potential [29] that takes this into account

$$U^{(l)}_{eff}(r) = -\frac{Z_l(r)}{r} - \frac{\alpha\left(1-\exp\left(-(\frac{r}{r_0})^6\right)\right)}{2r^4}, \tag{3.9}$$

with

$$Z_l(r) = 1 + (z-1)\exp(-a_1 r) - r(a_3 + a_4 r)\exp(-a_2 r). \tag{3.10}$$

Where α is the dipole polarizability, z charge of the nucleus, and $Z_l(r)$ the radial charge. The terms $(a_1, a_2, a_3, a_4, r_0)$ are experimental parameters [30, 31] that must be fitted well in order to obtain the right solutions of the Schrödinger equation.

After having the right form of $U_{eff}^{(l)}(r)$ we then solve the Schrödinger equation

$$\left(-\frac{1}{2}\partial_r^2 + U_{(eff)}^{l}(r) + \frac{l(l+1)}{2r^2}\right) g_{nl}(r) = E_n g_{nl}(r), \tag{3.11}$$

numerically. The potential is so complicated that analytical solutions look impossible thus leaving numerics as the only alternative.

This is achieved through space discretization by dr and writing the Hamiltonian in matrix form, the diagonalization of which gives the radial part of the eigenstates necessary for the numerical calculations to come. The angular part of the total wavefunction is taken to be the same as that of Hydrogen atom, equation 3.7, since it isn't affected by the modified potential.

The values used for the parameters in $U_{eff}^{(l)}(r)$ for this thesis are from [32].

The eigenenergies also are slightly affected, for the lower lying states, by $U_{eff}^{(l)}(r)$ and are given by [1]

$$E_{l,j} = -\frac{1}{(n - \delta_{l,j}(n))^2}, \tag{3.12}$$

where $\delta_{l,j}(n) = \delta_{l,j,0} + \frac{\delta_{l,j,2}}{(n-\delta_{l,j}(n))^2}$ is the quantum defect that accounts for the overlap between the Rydberg electron's wavefunction and that of the core electrons, it becomes quite negligible for high-lying Rydberg states [30, 31].

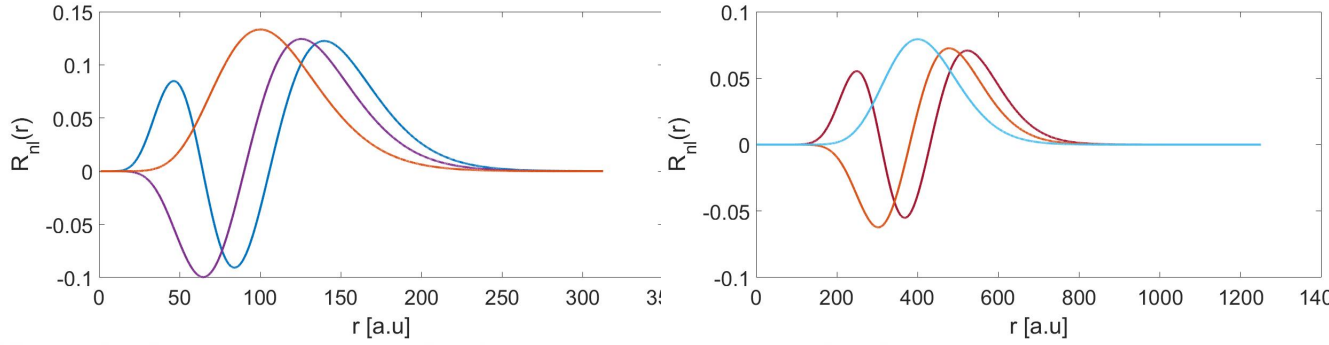

Figure 3.1: Sample Circular Wavefunctions $(n, l = n-1, m = n-1)$ from the Numerical solutions for: (a) n=10 , l=9 (orange), l=8 (violet) and l=7 (green) . (b) n=20, l=19 (light-green), l=18 (orange) and l=17 (magenta).

Surprisingly, the wavefunctions of the circular states when plotted, figure 3.1, resemble those of a three-dimensional harmonic oscillator, with the most circular state $(n, l = n-1, m = n-1)$ corresponding to the well-known gaussian-like ground state of the Harmonic oscillator having zero nodes on the position axis.

This particular *harmonic oscillator-like* nature of the circular states' wavefunctions will later help us with analytical manipulations of these wavefunctions. Before that, we will have a look at how these Alkali atoms interact.

3.1.1 Interactions between Rydberg Alkali atoms

The true exotic nature of Rydberg atoms becomes apparent when the interaction between the atoms dominates over their kinetic energies as is the case in ultra-cold physics [33]. Here, the interaction becomes the agent behind quantum mechanical phenomena such as dipole blockade [8], Rydberg aggregates [34] and others, that arise at ultra-cold temperatures. It is through these interactions that manipulation and control of the atomic samples is achieved [35], a detailed look at them is therefore of primary importance to us.

Consider two alkali atoms, say Rubidium, centred at positions 1 and 2, each with a valence electron at positions **a** and **b**, and separated by **R**.

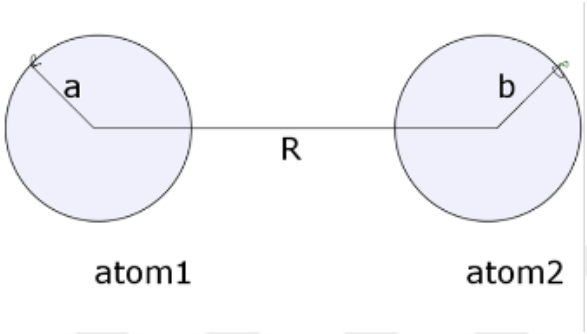

Figure 3.2: Two interacting Alkali Rydberg atoms

To avoid overlap of the wavefunctions of these electrons $|\mathbf{R}|$ is assumed to be far larger than both $|\mathbf{a}|$ and $|\mathbf{b}|$. This assumption is valid since a typical separation of $15\mu m$ is still much larger than $0.5\mu m$, radius of a Rydberg atom in n=100.

The two nuclei interact repulsively with each other and attractively with each other's Rydberg electron. Also the electrons interact repulsively with each other. This interaction can be written, with the separation vector taken to be directed from atom 1 to atom 2, as

$$V(\mathbf{R},\mathbf{a},\mathbf{b}) = \frac{1}{|\mathbf{R}|} - \frac{1}{|\mathbf{R}+\mathbf{b}|} - \frac{1}{|\mathbf{R}-\mathbf{a}|} + \frac{1}{|\mathbf{R}-(\mathbf{a}-\mathbf{b})|}. \tag{3.13}$$

This expression can then be simplified using binomial expansion in powers of $\frac{b}{R}$ or $\frac{a}{R}$ as, for example

$$\frac{1}{|\mathbf{R}+\mathbf{b}|} = \frac{1}{\sqrt{R^2+b^2+2\mathbf{R}.\mathbf{b}}} = \frac{1}{R}\left[1+\left(\frac{b^2}{R^2}+\frac{2\mathbf{R}.\mathbf{b}}{R^2}\right)\right]^{\frac{-1}{2}}, \tag{3.14}$$

$$= \frac{1}{R}\left[1-\frac{1}{2}\left(\frac{b^2}{R^2}+\frac{2\mathbf{R}.\mathbf{b}}{R^2}\right)+\frac{3}{8}\left(\frac{b^2}{R^2}+\frac{2\mathbf{R}.\mathbf{b}}{R^2}\right)^2\right]. \tag{3.15}$$

By expanding all the other terms in the interaction and dropping terms of order $(a/R)^2$, $(b/R)^2$ and adding up the rest, see **Appendix** A, one gets

$$V(\mathbf{R}, \mathbf{a}, \mathbf{b}) = \frac{\mathbf{a}.\mathbf{b}}{R^3} - 3\frac{(\mathbf{a}.\mathbf{R})(\mathbf{b}.\mathbf{R})}{R^5}. \tag{3.16}$$

To get a qualitative understanding of the nature of these interaction at separations considered small or large compared to some "critical radius"[1], we will be using only

$$V(\mathbf{R}, \mathbf{a}, \mathbf{b}) = \frac{\mathbf{a}.\mathbf{b}}{R^3}, \tag{3.17}$$

as the other term doesn't bring anything new [36] to the model in use.

3.1.2 Three-level atom example

In order for us to gauge the strengths and nature of the interactions between Rydberg atoms we consider a situation in which the atoms are assumed to have three levels $|s\rangle$, $|p\rangle$ and $|p'\rangle$. A non-vanishing matrix element of the dipole operator between $|s\rangle$ and $|p\rangle$, and $|s\rangle$,$|p'\rangle$ exist.

The following pair states then are available to be used as base kets [$|ss\rangle$, $|sp\rangle$, $|sp'\rangle$, $|pp\rangle$, $|ps\rangle$, $|pp'\rangle$, $|p'p'\rangle$, $|p's\rangle$, $|p'p\rangle$]. Define the system's Hamiltonian as

$$H(R) = H_{atom1} + H_{atom2} + V_{atom1-atom2}(R), \tag{3.18}$$

[1] Also called the van-der-Waals radius R_{vdW}.

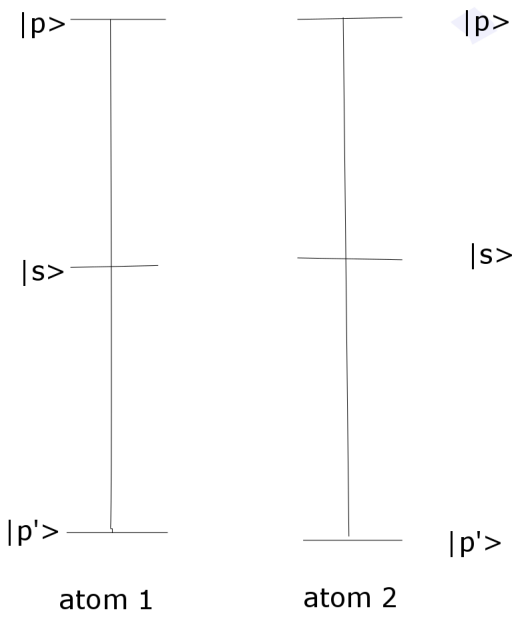

Figure 3.3: Three-level atom example

where $V_{atom1-atom2}(R)$ is eqn(3.17). Define the following

$$|\psi\rangle \in [|s\rangle, |p\rangle, |p'\rangle]; \mathbf{r} \in [\mathbf{a}, \mathbf{b}]; \langle\psi|a|\psi\rangle = \langle\psi|b|\psi\rangle = 0; \tag{3.19}$$
$$\langle s|\mathbf{r}|p\rangle = \mathbf{r}_+; \langle s|\mathbf{r}|p'\rangle = \mathbf{r}_-; \langle ss|H(R)|ss\rangle = 0, \langle pp|H(R)|pp\rangle = E_{++};$$
$$\langle p'p'|H(R)|p'p'\rangle = E_{--}; \langle pp'|H(R)|pp'\rangle = E_{+-};$$
$$|E_{++}|, |E_{--}| \gg |E_{+-}|.$$

Thus the states $|pp\rangle$, $|p'p'\rangle$ are energetically far away and therefore have minimum contribution. Using $|pp'\rangle$ and $|p'p\rangle$ we can then form a symmetric and anti-symmetric superposition as

$$|0\rangle = \frac{1}{\sqrt{2}}\Big(|pp'\rangle + |p'p\rangle\Big) \tag{3.20}$$
$$|1\rangle = \frac{1}{\sqrt{2}}\Big(|pp'\rangle - |p'p\rangle\Big),$$

these, together with $|ss\rangle$, can then be used to form the Hamiltonian matrix.

$$\langle 1|H(R)|ss\rangle = 0; \langle 1|H(R)|0\rangle = 0; \tag{3.21}$$

the $|1\rangle$ state can further be removed leaving only $|ss\rangle$ and $|0\rangle$ to work with.

$$\langle ss|H(R)|ss\rangle = 0; \langle 0|H(R)|0\rangle = E_{+-}; \tag{3.22}$$
$$\langle ss|H(R)|0\rangle = \frac{\sqrt{2}r_+r_-}{R^3} = \frac{d^2}{R^3};$$

with $|\mathbf{r}_+| = r_+$, $|\mathbf{r}_-| = r_-$, $d^2 = \sqrt{2}r_+r_-$ and $E_{+-} = -\Delta$, we then have

$$H(R) = \begin{pmatrix} 0 & \frac{d^2}{R^3} \\ \frac{d^2}{R^3} & -\Delta \end{pmatrix}, \tag{3.23}$$

by diagonalizing $H(R)$ we find the eigenvalues corresponding to the interactions as

$$E_{\pm}(R) = \frac{\Delta}{2}\left[-1 \pm \sqrt{1 + \left(\frac{2d^2}{\Delta R^3}\right)^2}\right]. \tag{3.24}$$

To see the nature of the interactions check the limit at which the squared term under the square root is far less than 1 and far greater than 1, that is

- When $\left(\frac{2d^2}{\Delta R^3}\right) \ll 1$
  $E_{\pm}(R) = \frac{\Delta}{2}\left[-1 \pm 1 + \frac{1}{2}\left(\frac{2d^2}{\Delta R^3}\right)^2\right] \propto \frac{1}{R^6}$, which is **van-der-Waals** in nature.
- $\left(\frac{2d^2}{\Delta R^3}\right) \gg 1$
  $E_{\pm}(R) = \frac{\Delta}{2}\left[\frac{2d^2}{\Delta R^3}\right] \propto \frac{1}{R^3}$, which is **Dipole-dipole** in nature.
- The critical radius, van-der-Waals radius, here then is
$$\left(\frac{2d^2}{\Delta R^3}\right)^2 = 1 \rightarrow R_c = \left(\frac{2d^2}{\Delta}\right)^{1/3}. \tag{3.25}$$

For separations smaller than R_c the interaction potential is dipole in nature and is given by $E(R) = \frac{C_3}{R^3}$ with C_3 the dipole dispersion coefficient that determines the strength of the dipole matrix elements.

For separations larger than R_c the interaction potential is van-der-Waals in nature and given by $E(R) = \frac{C_6}{R^6}$.

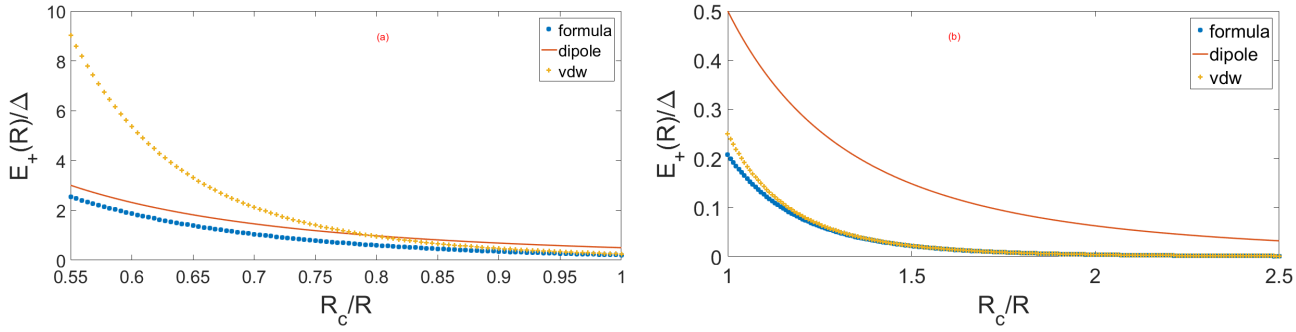

Figure 3.4: The resulting interaction between two Rydberg atoms when: [a] $R < R_c$ (red and blue) Dipole-dipole. [b] $R > R_c$ (blue and yellow) van-der-Waals.

The dipole-dipole interactions are generally resonant as they relate to resonantly coupled states, while the van-der-Waals interactions involve both resonant and off-resonantly coupled states, resulting in larger Hilbert spaces, big-sized Hamiltonians.

A typical example of a resonant dipole-dipole interaction is the $|sp\rangle$ and $|ps\rangle$ coupling, while that of an off-resonant van-der-Waals is the $|ss\rangle$, $|pp\rangle$ coupling.

The dipolar and van-der-Waals nature of equation 3.16 at varying separations could also be shown using perturbation theory, where in first-order one gets the $\propto \frac{1}{R^3}$ dipole-dipole interaction, and in second-order $\propto \frac{1}{R^6}$ van-der-Waals.

3.1.3 Potential calculation: code summary

To solve the time-independent Schrödinger equation 3.18, the numerical code used for this thesis starts by choosing a range of quantum numbers (n, l), states, setting up a matrix representation of the interacting Hamiltonian in this restricted Hilbert space. We also exploit that $M = m_1 + m_2$, where $m_j = -l \rightarrow l$, is conserved along the quantization axis.

Convergence is reached when for different range of (n, l) the same result is found. After this, a restricted Hilbert space where the lowest possible range that puts the state of interest in the middle, say $[(n-2) : (n+2)]$, and takes less running time is chosen.

A set of all possible states that satisfy the m conservation are then chosen and used to determine the size of the Hamiltonian matrix and its matrix elements using equation 3.18.

The found Hamiltonian is then diagonalized to find its eigenstates and eigenenergies, with the eigenstates being a superposition of the coupled two-atom states, and the eigenenergies corresponding to equation 3.12 and representing the interaction potentials.

We use this code for three purposes: [1] calculations of van-der-Waals interactions involving circular Rydberg states, see section 3.2.3, [2] extraction of dipole-dipole transition matrix elements as well as [3] extraction of few state Hamiltonians for the time-dependent study of transport when not starting in an eigenstate, see section 3.2.

3.2 Numerics: Scalings, Populations and Angular momentum transfer

Here, we present the numerical results of our work on circular Rydberg states. We start with the resonant dipole-dipole and move on to the van-der-Waals interactions.

3.2.1 The resonant on-axis case: Dipole-dipole

In the resonant on-axis case one of the atoms occupies the state $|a\rangle = |n, l = n-1\rangle$ and the other $|b\rangle = |n, l = n-2\rangle$. The atomic centres are aligned along

the quantization axis, so that for the states in hand we demand that $(m_1 = n-1) + (m_2 = n-2)$ be conserved, only the states satisfying this condition couple.

The dynamics is quite simple: one of them starts in $|a\rangle$ and the other in $|b\rangle$, the one in $|a\rangle$ then de-excites to $|b\rangle$ by transferring its angular momentum to the one in $|b\rangle$ which then resonantly excites to $|a\rangle$ and vice-versa.

From the dipole Hamiltonian we extract the off-diagonal element and use it in $V_{dipole} = \frac{C_3}{R^3}$ to find C_3, which determines the strength of the dipole coupling between the circular states.

To determine the dipole coupling scaling with n we use the values given in Table 3.1. Here, various combinations of the C_3 s with their n s are used to arrive at a common scaling for a general case. To do this we start from

$$C_3 = C^{(0)} n^{\alpha}, \tag{3.26}$$

where n is the principal quantum number of the used states, $C^{(0)}$ dispersion term common to all considered states, α the strength with respect to n and C_3 the dipole dispersion coefficient whose strength, scaling, with n we intend to find.

For different n values one then solves the equation

$$\left[\frac{C_3^{(1)}}{C_3^{(2)}}\right] = \left[\frac{n^{(1)}}{n^{(2)}}\right]^{\alpha} \rightarrow \alpha = \frac{\log\left[\frac{C_3^{(1)}}{C_3^{(2)}}\right]}{\log\left[\frac{n^{(1)}}{n^{(2)}}\right]}, \tag{3.27}$$

where α is the scaling with n. So that for n=20 and n=40, $\alpha = \frac{\log\left[\frac{15.907}{130.60}\right]}{\log\left[\frac{20}{40}\right]} = 3.0375$.

We have calculated and checked the values of α for other combinations as well, and conclude that the dipole coupling between neighbouring circular states scales as n^3.

Numerical results for R=4μm		
n	V_{dipole} [au]	C_3[MHz μm^3]
10	4.4746×10^{-12}	1.8837
20	3.7786×10^{-11}	15.907
30	1.2970×10^{-10}	54.600
40	3.1024×10^{-10}	130.60
80	2.5138×10^{-9}	1058.2

Table 3.1: Numerical results of resonant-on axis dipole-dipole potential for R=4μm.

3.2.2 Populations and Angular momentum transfer: Time evolution

Here we examine, through time-evolution, how populations are transferred using circular states, by solving the time-dependent schrödinger equation,

$$i\partial_t|\psi(t)\rangle = H|\psi(t)\rangle, \tag{3.28}$$

where $|\psi(t)\rangle$ is the state of interest and H the dipole Hamiltonian obtained as explained in the previous section, with $|(n, n-1, n-1), (n, n-2, n-2)\rangle$ as initial state.

Sample plot of populations $= |\psi(t)|^2$ against t[μs] for $n = 40$ is given below:

As figure 3.5 shows, a completely-resonant transfer of population between the states is possible with period ranging in the μs. This result gives hope that the angular momentum also could be resonantly transferred between the atoms.

A quick look at the plots for other n values gives the following as the periods with which the transfers happen:

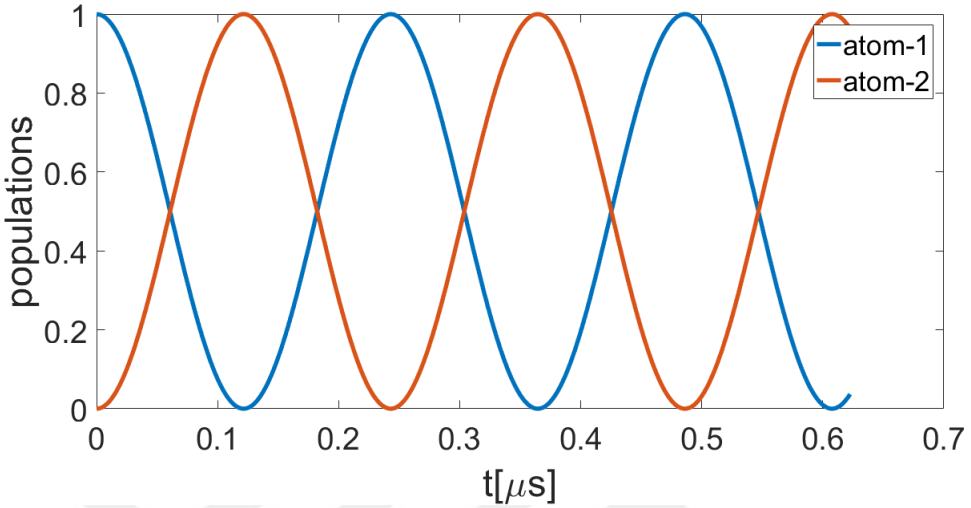

Figure 3.5: Population transfer using circular states for R=4μm and n=40 .

Transfer periods for R=4μm	
n	t[μs]
10	16 ± 0.5
20	2 ± 0.2
40	0.25 ± 0.02
80	0.03 ± 0.002

Table 3.2: Population transfer periods with circular states.

By using equation 3.27 and replacing the C_3 s with the respective periods, we find the transfer period scaling for n=10 and n=20, $\alpha = \frac{\log\left[\frac{16}{2}\right]}{\log\left[\frac{10}{20}\right]} = -3$.

The population transfer period therefore scales as n^{-3}.

Analytical calculation of these periods is also possible when the form of the dipole potential used in the time-evolution is used, one such form is

$$H_{dip} = \frac{\Omega}{2}\left[|a\rangle\langle b| + |b\rangle\langle a|\right], \tag{3.29}$$

where Ω is the coupling frequency. Since the off-diagonal elements in our

Hamiltonian 3.28 matrix represent the dipole terms, we can directly equate them to the terms above so that

$$V_{dip} = \frac{\Omega}{2} \rightarrow \Omega = 2V_{dip}, T = \frac{2\pi}{\Omega} \rightarrow T = \frac{\pi}{V_{dip}}. \tag{3.30}$$

where T is the period. Using the V_{dip} in 3.1, with $1[au] = 2.4 \times 10^{-11}\mu s$, we get the following:

for n=10, $T = \frac{\pi}{4.4746 \times 10^{-12} au} = 16.850\mu s$.

Those of the others follow in a similar way as tabulated below.

Transfer periods for R=$4\mu m$		
n(npick)	$t_{numeric}[\mu s]$	$t_{analytic}[\mu s]$
10	16 ± 0.5	16.850
20	2 ± 0.2	1.9954
40	0.25 ± 0.02	0.2430
80	0.03 ± 0.002	0.0300

Table 3.3: Analytical and numerical results for the population transfer periods with circular states.

Next we show how the angular momentum transfer can be connected to the just discussed population transfer.

In the case of our two atoms, we would want to know their angular momenta in the initial state $|(n, n-1, n-1), (n, n-2, n-2)\rangle$ so that over the course of their interaction, for some time t, we can compute the amount transferred by each atom to the other.

We start by defining some state $|\psi(t)\rangle$ as

$$|\psi(t)\rangle = \sum_k C_k(t)|k\rangle, \tag{3.31}$$

where $|k\rangle$ is an atomic eigenstate. The expectation value of L in this state then is

$$\langle\psi(t)|L|\psi(t)\rangle = L_{exp} = \sum_{n,k} |C_k(t)|^2 \sqrt{l_k^{(n)}(l_k^{(n)}+1)}, \tag{3.32}$$

with n labelling the atoms while k labels the state. These $|C_k|^2$ s are the populations whose change with time we plotted in Figure 3.5. This way we can write each atom's angular momentum at any time as

$$L_{atom1} = |C_0(t)|^2 \sqrt{l_0^{(1)}(l_0^{(1)}+1)} + |C_1(t)|^2 \sqrt{l_1^{(1)}(l_1^{(1)}+1)}. \tag{3.33}$$

$$L_{atom2} = |C_0(t)|^2 \sqrt{l_0^{(2)}(l_0^{(2)}+1)} + |C_1(t)|^2 \sqrt{l_1^{(2)}(l_1^{(2)}+1)}. \tag{3.34}$$

We then choose a pair of circular states occupied by the atoms and monitor how L changes with time. The results of our simulations from 3.5 and 3.1 are used here to look at L.

Looking at figure 3.6 one realizes that the transfer is resonant and periodic.

The case considered so far where the populations, energy and angular momentum are being resonantly and periodically transferred between the two atoms when their nuclei are perfectly aligned is too ideal since the atoms are expected to be randomly distributed within their trapping regions. As a result in section 3.3 we consider a more realistic case in which the atomic nuclei are some degrees off the quantization axis and try to see how that affects the results obtained so far.

Another case to look at is one in which the two atoms not only occupy states with different angular momenta but also energy, the initial state being something like $|(n, n-1, n-1), (n+1, n, n)\rangle$. The atoms here not only have to deal with

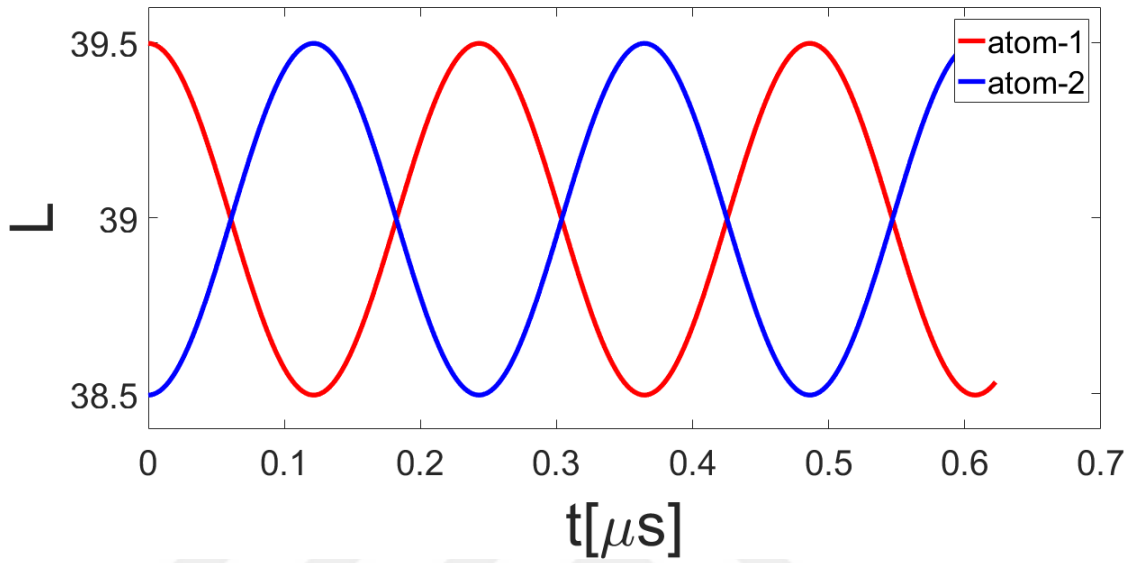

Figure 3.6: Angular momentum transfer with atoms in circular Ryberg states separated by R=4μm in n=40.

their different angular momenta but also energies[2]. Following same procedure as the previous section we obtain the following results

Numerical results for two atoms in $\|(n, n-1, n-1), (n+1, n, n)\rangle$		
n	V_{dipole} [au]	C_3[MHz μm^3]
20	9.2634×10^{-11}	7.6189×10^1
30	4.6553×10^{-10}	3.8289×10^2
40	1.4657×10^{-9}	1.2055×10^3
50	3.5700×10^{-9}	2.9362×10^3

Table 3.4: Numerical results for dipole coupling coefficients between atoms in different energy and angular momentum states for R=5μm

.

and the scaling as usual for $n = 30$ and $n = 50$, $\alpha = \frac{\log\left[\frac{38.289}{293.62}\right]}{\log\left[\frac{20}{50}\right]} = 3.9879$. It scales as n^4 as compared to n^3 for atoms in states with same energy but different angular

[2]In the previous case the energy levels are the same so that the resonant nature of population transfer gives also resonant $|L|$.

momenta. One particular case we are quite interested in, is finding a pair of such circular states, $|(n, n-1, n-1), (n-1, n-2, n-2)\rangle$,$|(n, n-1, n-1), (n+1, n, n)\rangle$ and $|(n, n-1, n-1), (n, n-2, n-2)\rangle$, having almost the same C_3 coefficients. Such pairs of states might then allow information transport through successive collisions between Rydberg atoms as shown in [24]. This in turn may be a useful addition of a data-bus (flying qubits [37, 38, 39]) for Rydberg based quantum computing [11].

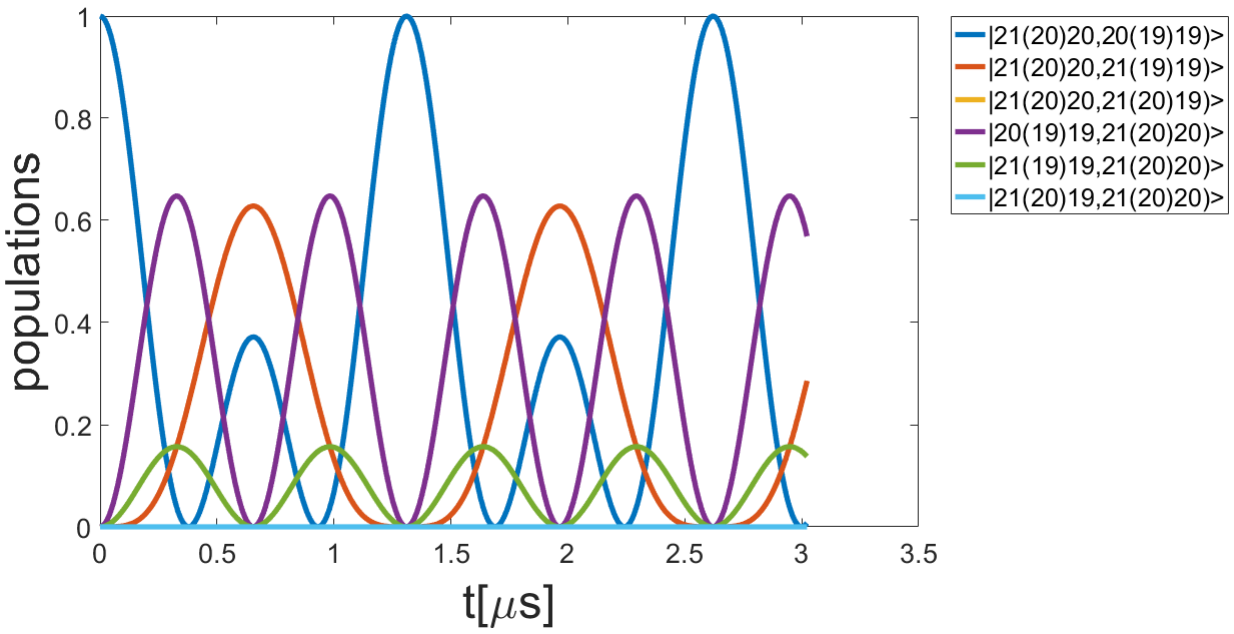

Figure 3.7: Results of population transfer with circular states starting in $|(n, n-1, n-1), (n+1, n, n)\rangle$

.

For the energy and angular momentum transfer of Table 3.4, it suffice to look at the population transfer. Here we look at only for $n = 20$ from the table, as shown in 3.7.

Here, the atoms start in $|21(20)20, 20(19)19)\rangle$ (blue) and, in the time $0 < t < 0.5\mu s$, transfer around 63% of their E and L to $|20(19)19, 21(20)20)\rangle$ (magenta) in which case both their E and L states resonantly change, 23% to $|21(20)20, 21(19)19)\rangle$ (red), and 14% to $|20(19)19, 21(20)20)\rangle$ (green).

Then at t $\approx$ $0.7\mu s$ these 63% (magenta) and 14% (green) completely empty-up to give around 65% to $|21(20)20, 21(19)19)\rangle$ (red) and 35% to $|21(20)20, 20(19)19)\rangle$ (blue). The steps of $0 < t < 0.5\mu s$ are then repeated in reversed order. All the states then transfer their E and L to the initial state $|21(20)20, 20(19)19)\rangle$ thus reaching a full period.

So, the transfer over a full period happen, with no loss, is resonant, and only happen to the completely circular two-atom states.

Unfortunately, the presence of transfer to other circular states instead of only the two we are interested in, rules out such pair state as candidates to use as data-bus.

3.2.3 Van-der-Waals interactions

The general assumptions, the atomic centres being on-axis, the existence of resonant/off-resonant couplings between states and such, made in the previous sections still hold here. One major difference is that the inter-atomic separations here are larger and the atoms are in same initial states which we chose to be our initial state in the simulations. The nature of couplings between states is mixed, some are resonant and some are not, and the Hamiltonian matrix is generally huge.

To find the van-der-Waals coefficient C_6 and its scaling one must then use some kind of fitting scheme. Here, we fit the eigenvalues of the Hamiltonian to some polynomial and extract the coefficient of $1/R^6$. To do the van-der-Waals scaling we use equation 3.27 and replace C_3 with C_6 so that

Numerical results for R=12μm	
n	C_6[au]
20	5.5478×10^{14}
30	7.8114×10^{16}
35	5.0705×10^{17}
40	2.5547×10^{18}

Table 3.5: Numerical results of van-der-Waals coefficient between two atoms for R=12μm

.

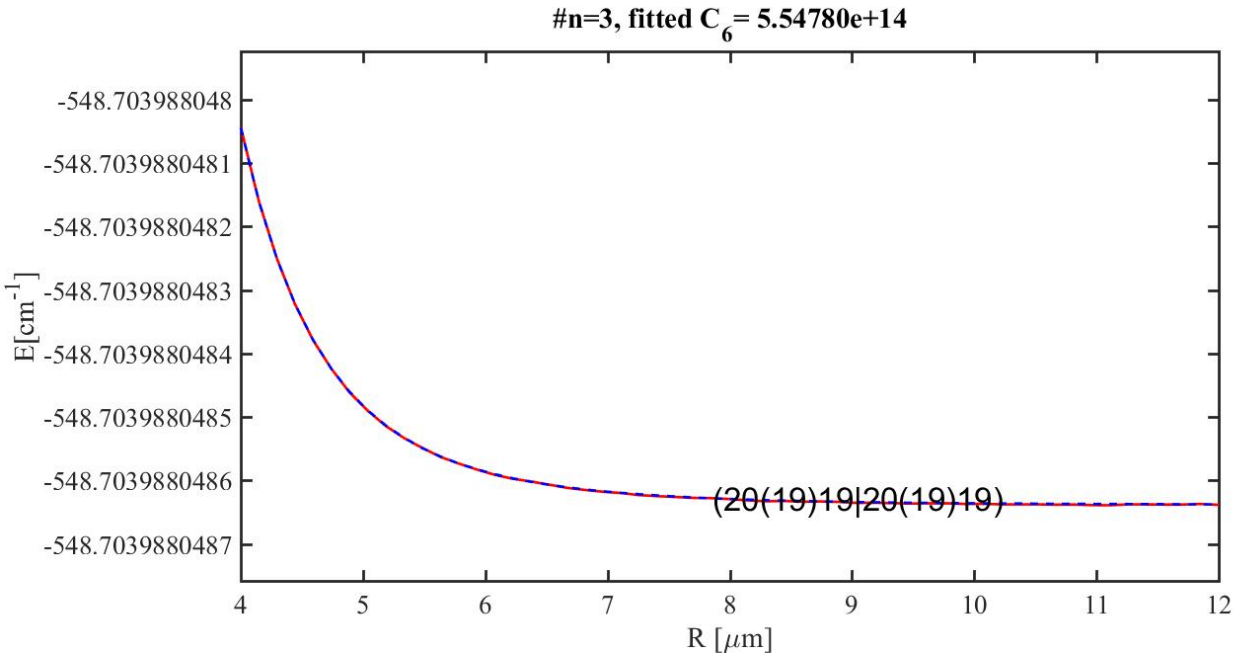

Figure 3.8: Plot of the fitted van-der-Waals curve for two atoms in $|(n, n-1, n-1), (n, n-1, n-1)\rangle$ with R=12μm.

for n=30 and n=35, $\alpha = \frac{\log\left[\frac{7.8114}{50.705}\right]}{\log\left[\frac{30}{35}\right]} = 12.1336$.

One concludes then that it scales as n^{12} as expected. [3]

[3] the value converges to 12 as larger n values are chosen.

3.3 The Off-axis case: Angular momentum transfer/loss

Here the inter-atomic axis is some degrees off the previously assumed 'quantization axis' so that the projection of L is no longer conserved along it any more. The aim then is to see how this affects the obtained results so far.

The results for $n = 10$ R=5μm, with the initial state $|(10, 9, 9), (10, 8, 8)\rangle$ are presented below :

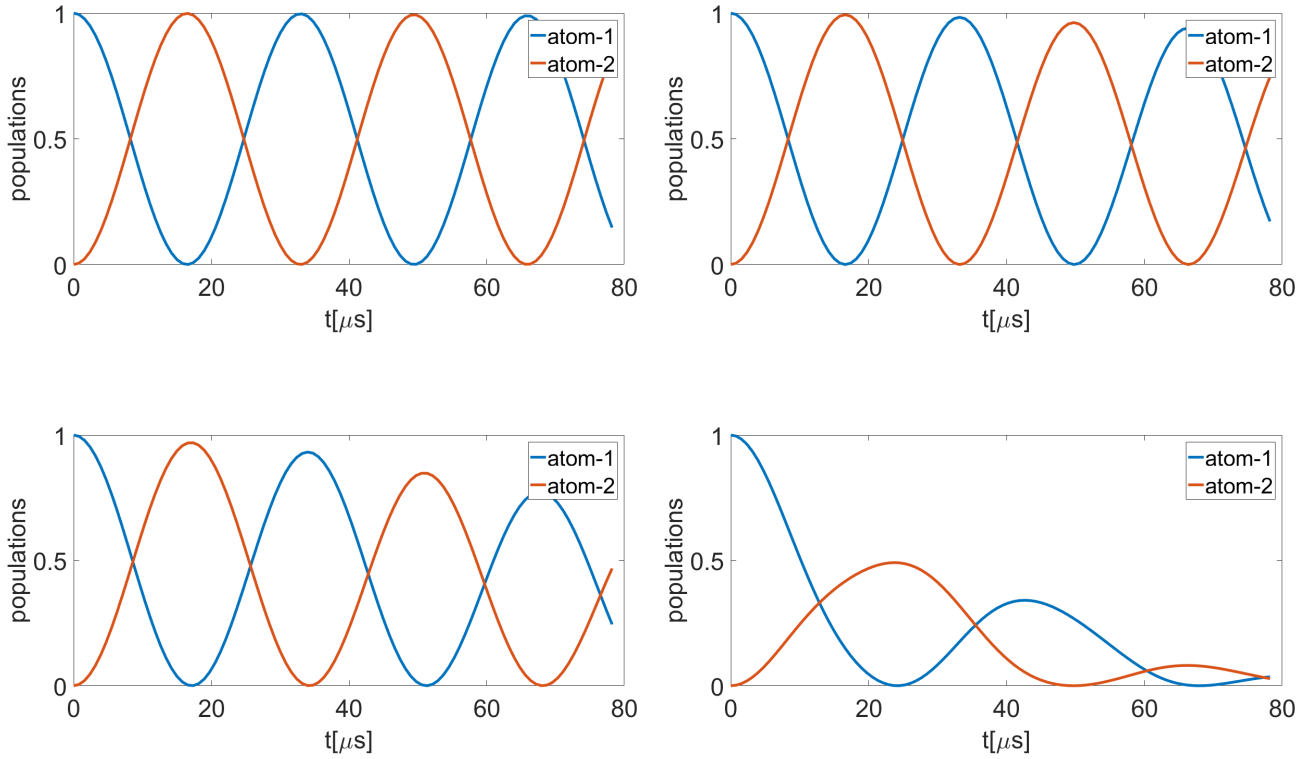

Figure 3.10: Population transfer when the inter-atomic axis is off by [a] 2° [b] 5° [c] 10° [d] 30°

.

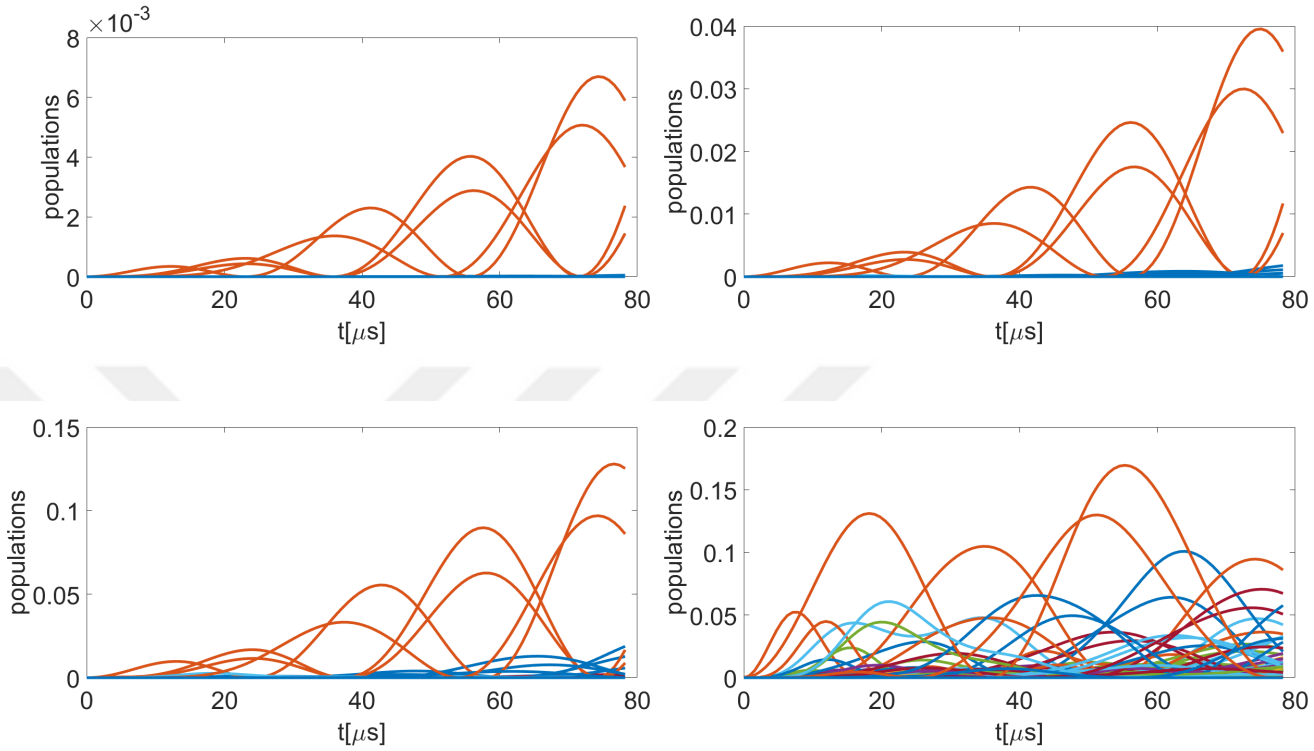

Figure 3.12: Population in undesired states when the inter-atomic axis is off by [a] 2° [b] 5° [c] 10° [d] 30°.

Using the results of figure 3.10 we can interpret the L and E transfer using these states when oriented at some angle α off the quantization axis as follows: For $\alpha = 2°$ '[a]' around 99% of the transfer is achieved during the first period and a loss of 1% to 2% is recorded in subsequent periods that increase due to the loss. This lost L and E and how it is distributed is shown in figure 3.12 '[a]'. With this, one successfully achieves desirable transfer of up to 98% in as long as $50\mu s$.

For $\alpha = 5°$ around 97% transfer is achieved in the first period with losses of 3-4% in subsequent periods, a maximum of 95% transfer is possible in $50\mu s$. The resulting losses can be seen in graph '[b]'of figure 3.12.

For $\alpha = 10°$ the transfer starts to get quickly damped, with as much as 15% loss recorded in 50 μs and more than 50% in the next 40 μs. Still as much as 91% transfer could be achieved in the first 30-35μs. The loss from this part is shown in '[c]' of figure 3.12.

When the angle gets as large as 30° the transfer after some time becomes non-existent. In fact, more than 60% is lost after 40 μs and by the time we get to 90 μs there is nothing left to transfer. This loss, of course, benefits the other states outside of the ones in question as they share among them the lost L and E as shown in '[d]' of figure 3.12.

The take-away here then is that with proper trapping of the atoms, resulting in small α, reasonable transfer could be achieved in times shorter than the life-times of these circular states. With the varieties of trapping techniques available today [40, 41, 42, 43] achieving small α s, or alternately carrying out the desired operations before the loss begins, should be possible.

3.4 Analytical Results

Here we look at a possible analytical result for the circular states used in this study. To do this we use [44]

$$V = -8\pi\sqrt{\frac{2\pi}{15}}\frac{(d_{n_a l_a, n_b l_b})^2}{R^3}\sum_{\mu=2}^{-2} Y^*_{2\mu}(\hat{R})\langle l_a m_a, l_b m_b|[Y_1(\hat{r_1})Y_1(\hat{r_2})]^\mu_2|l_b m'_b, l_a m'_a\rangle, \tag{3.35}$$

which is an explicit form of equation 3.16 when the total angular momentum connecting the two atom states is considered. $Y^*_{2\mu}(\hat{R})$ defines the inter-nuclear orientation of the atoms, $[Y_1(\hat{r_1})Y_1(\hat{r_2})]^\mu_2$ are the Clebsch-Gordan coefficients that connect the transformation between coupled basis to single atom basis, $|JM\rangle \rightarrow |j_1 m_1, j_2 m_2\rangle$, and dipole element between states

$$d_{n_a l_a, n_b l_b} = \int_0^\infty r R_{n_a, l_a}(r) R_{n_b, l_b}(r)\, dr. \tag{3.36}$$

From equation 3.35 one understands that only states satisfying $|l_a - l_b| = 1$ result in non-zero elements.

To use this expression we choose our circular states and find the corresponding $R_{n,l}(r)$ and $Y^m_l(\theta, \phi)$ which we use in finding V. So, for atom 1 ($n, l = n-1, m =$

$n-1$) and atom 2 ($n, l = n-2, m = n-2$), using equation 3.6, see **Appendix** B, we have

$$R_{(n,n-1)}(r) = \sqrt{(\frac{2}{n})^3 \frac{1}{2n(2n-1)!}} \left(\frac{2}{n}\right)^{n-1} \left(r^{n-1} exp(-\frac{r}{n})\right), \tag{3.37}$$

$$R_{(n,n-2)}(r) = \sqrt{(\frac{2}{n})^3 \frac{1}{2n(2n-2)!}} \left(\frac{2}{n}\right)^{n-2} \left(r^{n-2} exp(-\frac{r}{n})\right) \left((2n-2) - \frac{2r}{n}\right), \tag{3.38}$$

and from equation 3.7

$$Y^{(n-1)}_{(n-1)}(\theta,\phi) = \frac{(-1)^{n-1}}{2^{n-1}(n-1)!} \sqrt{\frac{(2n-2)!(2n-1)}{4\pi}} \left(\sin(\theta) exp(i\phi)\right)^{n-1}, \tag{3.39}$$

$$Y^{(n-2)}_{(n-2)}(\theta,\phi) = \frac{(-1)^{n-2}}{2^{n-2}(n-2)!} \sqrt{\frac{(2n-4)!(2n-3)}{4\pi}} \left(\sin(\theta) \exp(i\phi)\right)^{n-2}. \tag{3.40}$$

And for $[Y_1(\hat{r_1})Y_1(\hat{r_2})]^{\mu}_2$ we make the $|JM\rangle \rightarrow |j_1 m_1, j_2 m_2\rangle$ transformation and pick the non-zero term when (θ, ϕ) are set to zero. This happens to be the $|2,0\rangle$ term given by

$$|2,0\rangle = \frac{1}{\sqrt{6}} \left(Y^{(1)}_{1,-1} Y^{(2)}_{1,1} + Y^{(1)}_{1,1} Y^{(2)}_{1,-1} + 2Y^{(1)}_{1,0} Y^{(2)}_{1,0}\right), \tag{3.41}$$

with $Y_{(1,\pm 1)}(\theta,\phi) = \mp\sqrt{\frac{3}{8\pi}} \sin(\theta) \exp(\pm i\phi)$ and $Y_{(1,0)}(\theta,\phi) = \sqrt{\frac{3}{4\pi}} \cos(\theta)$.

The term $\langle l_a m_a, l_b m_b | [Y_1(\hat{r_1})Y_1(\hat{r_2})]^{\mu}_2 | l_b m'_b, l_a m'_a \rangle$ then turns into an integral, with only the second term of equation 3.41 contributing to give

$$I = \int d\Omega_1 d\Omega_2 Y^{(1)*}_{n-1,n-1}(\theta_1,\phi_1) Y^{(2)*}_{n-2,n-2}(\theta_2,\phi_2) [|2,0\rangle] Y^{(1)}_{n-2,n-2}(\theta_1,\phi_1) Y^{(2)}_{n-1,n-1}(\theta_2,\phi_2), \tag{3.42}$$

with equations 3.39, 3.40, 3.41 used one gets

$$\begin{aligned} I = & \frac{(-1)^{2(2n-3)}(2n-1)(2n-3)(2n-2)!(2n-4)!}{2^{2(2n-3)}\left((n-1)!(n-2)!\right)^2} \\ & \times \left(\frac{1}{4\pi}\right)^2 \left(\frac{-3(2\pi)^2}{8\pi\sqrt{6}}\right) \left(\int_0^{\pi} (\sin(\theta))^{2n-1} \, d\theta\right)^2. \end{aligned} \tag{3.43}$$

And

$$d_{n_a l_a, n_b l_b} = \int_0^{\infty} r(rR_{n_a,l_a}(r))(rR_{n_b,l_b}(r)) \, dr = \frac{-3n}{2}\sqrt{(2n-1)}. \tag{3.44}$$

Putting everything together, with $Y^*_{2,0}(\hat{R}=\hat{Z})=\sqrt{\frac{5}{4\pi}}$, we get

$$V=\frac{-8\pi}{R^3}\sqrt{\frac{2\pi}{15}}\sqrt{\frac{5}{4\pi}}\left(\frac{-3n}{2}\sqrt{(2n-1)}\right)^2 \times\frac{(-1)^{2(2n-3)}(2n-1)(2n-3)(2n-2)!(2n-4)!}{2^{2(2n-3)}\left((n-1)!(n-2)!\right)^2} \times\left(\frac{1}{4\pi}\right)^2\left(\frac{-3(2\pi)^2}{8\pi\sqrt{6}}\right)\left(\int_0^{\pi}(\sin(\theta))^{2n-1}\,d\theta\right)^2, \tag{3.45}$$

this then we turn into Hamiltonian matrix. Following same procedure as the preceding sections, we obtain for the on-axis dipole-dipole case the following:

Analytical results for R=4μm			
n	V_{dipole} [au]	C_3[MHz μm^3]	T[μs]
10	4.685×10^{-12}	1.9723	16.093
20	3.956×10^{-11}	16.654	1.9059
30	1.3590×10^{-10}	57.211	0.5548
40	3.2480×10^{-10}	136.73	0.2321

Table 3.6: Analytical results of the on-axis case for R=4μm

The above obtained results agree with those of tables 3.1 and 3.2, thus validating the numerical results of the text in previous sections. Without performing any calculations it is safe to say that the C_3 for atoms in states with same energy but different angular momentum, scales as n^3 and the period of the populations transfer as n^{-3}.

3.5 Conclusion

Throughout this chapter we have studied circular Rydberg states and the dynamics and interactions between atoms in these states. We found that the radial part of circular states' wavefunctions show features akin to a $3D$ Harmonic oscillator with the most circular state corresponding to the Gaussian-like ground state. We

have also found that the interaction between atoms in these states are of different strengths compared to those in non-circular states.

Additionally we have studied the transfer of energy and angular momentum with atoms in these states. It was found that, for atoms in states with the same energy but different angular momenta and having nuclei perfectly aligned with the quantization axis, the transfer is completely resonant and lasts for as long a time as the lifetime of the states.

Also, by starting in circular states with different energy and angular momenta, it is always possible to return to the initial state after a full transfer period.

However, upon studying the off-axis case, we found that the transfer is significantly damped for angles bigger than 5° due to transfer to undesirable lower lying states which results in the decay of the circular states. Proper trapping of the atoms is of utmost importance here.

Chapter 4

Comparison between results

Having gone through classical, numerical quantum mechanical and analytical quantum mechanical treatment of angular momentum transfer between two atoms using circular Rydberg states, here, we compare the obtained results from these models.

4.1 Numerical - Analytical results comparison

Here, we make the comparison for two atoms separated by R=10μm in $|(40, 39, 39), (40, 38, 38)\rangle$. Figure 4.2 shows that the quantum mechanical results of the numerical model adopted during this study are in good agreement with the analytical results obtained in section 3.4, thus confirming the results of chapter **??**.

As a result, comparing the numerical(quantum mechanical) and classical results should give same results as the analytical(quantum mechanical) and classical comparison, this we chose to do here.

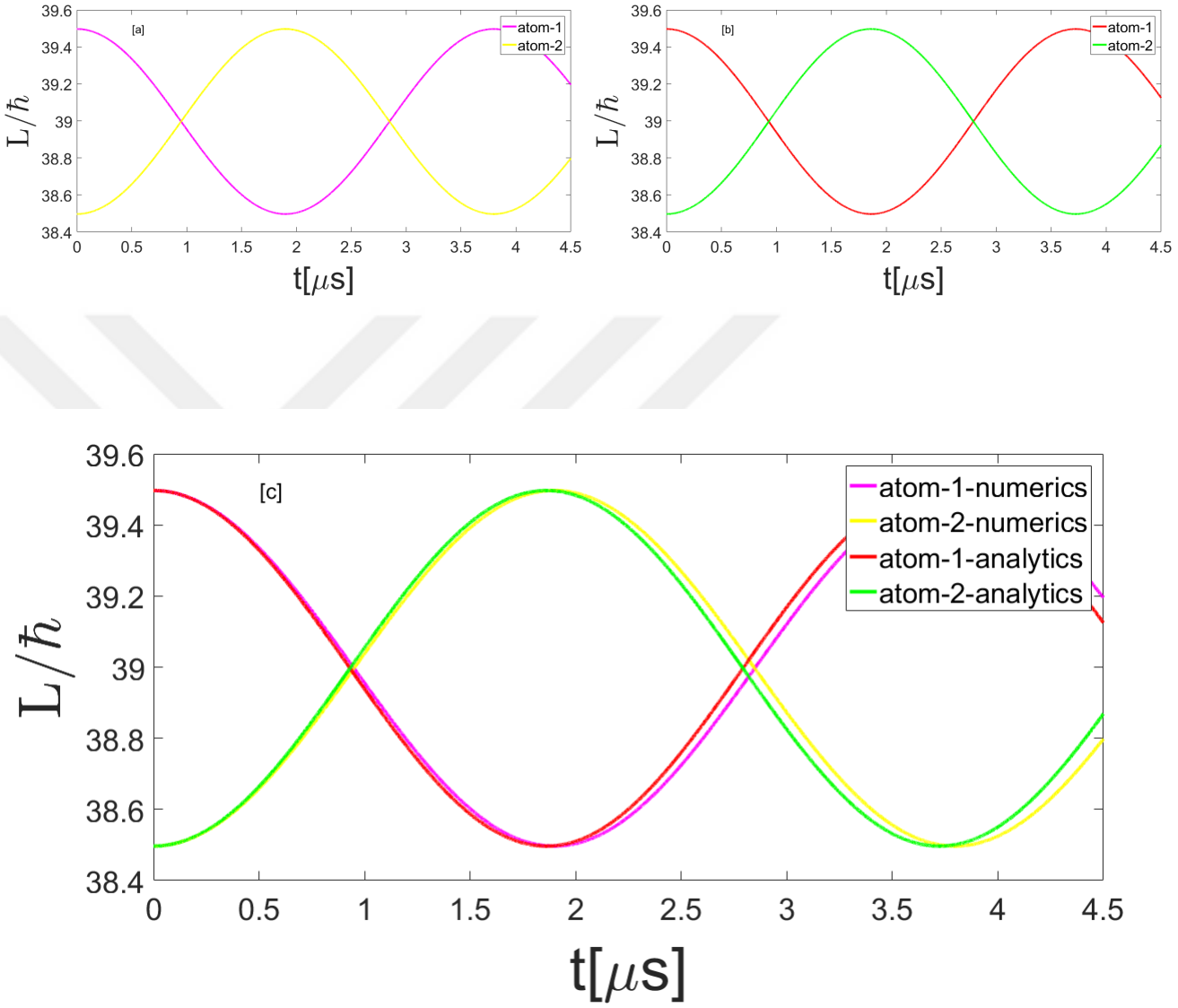

Figure 4.2: Comparison between quantum mechanical results of angular momentum transfer using Rydberg atoms separated by R=10μm in $|n, l, m\rangle \rightarrow |40, 39, 39\rangle$ and $|40, 38, 38\rangle$ [a] Numerical result [b] Analytical result [c] Numerical-Analytical comparison.

4.2 Quantum mechanical - Classical comparison

Here the atoms are in $|(80, 79), (80, 78)\rangle$, and separated by R=10$\mu m$.

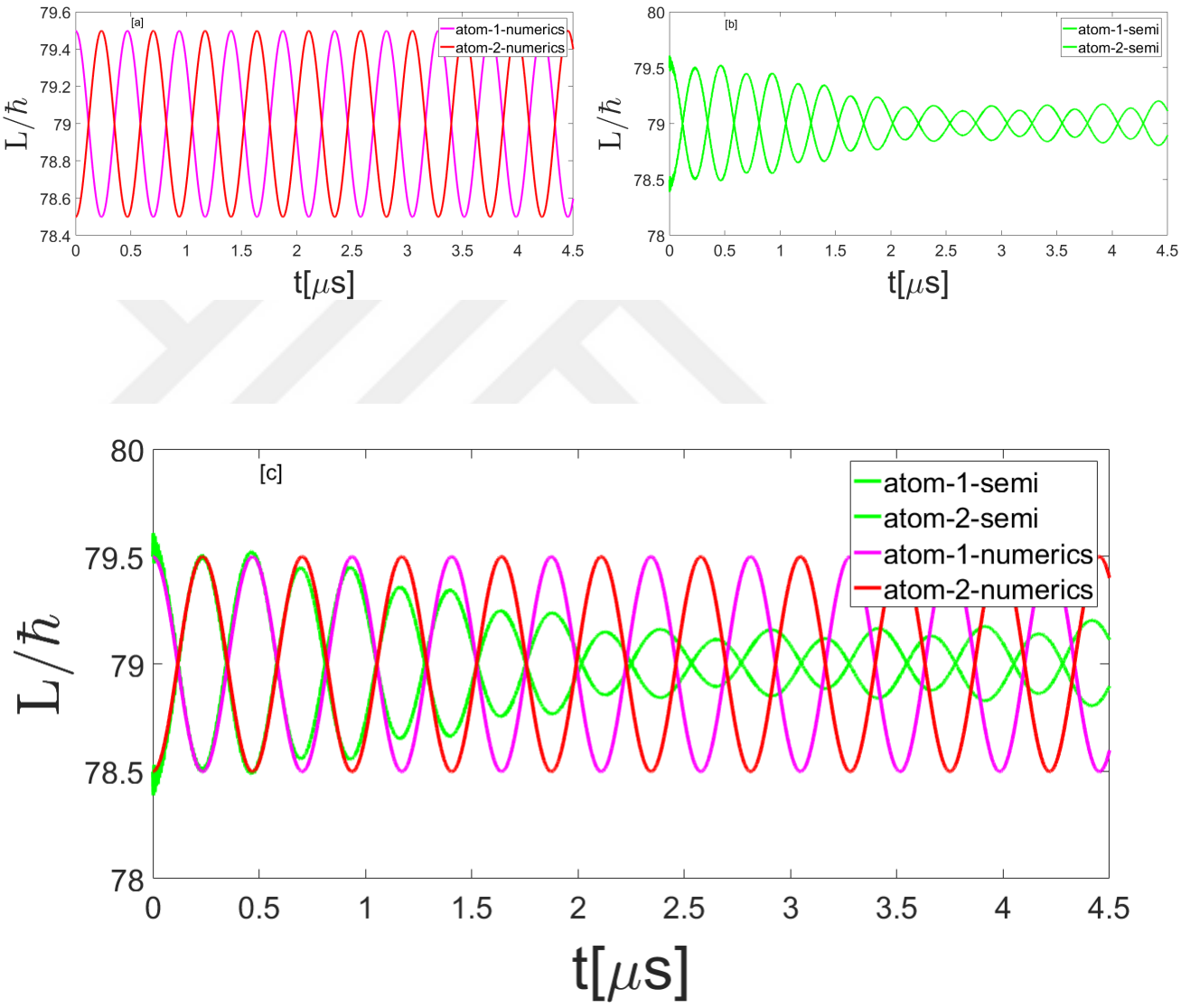

Figure 4.4: Comparison of angular momentum transfer using Rydberg atoms separated by R=10μm in $|n, l\rangle \rightarrow |80, 79\rangle$ and $|80, 78\rangle$ [a] Quantum mechanical result [b] Classical result [c] Quantum mechanical - Classical comparison.

As seen above, due to de-phasing the angular momentum transfer gets damped

for the classical model while the quantum mechanical one remains un-damped. Still, the two models agree with each other for $0 < t < 2.3\mu s$, after which due to increasing de-phasing the period of the classical transfer increases as the magnitude of the angular momentum transferred decays towards equilibrium, while the quantum mechanical results remain resonant and un-damped for all times.

The takeaway here then is that for a reasonably long time, on the atomic scale, the classical model works just as well, and if not for the de-phasing, the magnitude of the transferred angular momenta would have perfectly matched that of the quantum mechanical results, see above, thus providing a perfect agreement.

It would be interesting to investigate the origin of de-phasing in such classical systems in future projects.

4.2.1 Conclusion

We have seen, from the results of our comparisons, that the quantum mechanical models, numerical and analytical, agree very well with each other thus validating the assumptions made and/or results produced by them in previous chapters. We have also seen a great deal of agreement between the quantum mechanical and classical results for $0 < t < 2.3\mu s$, after which increasing de-phasing lengthens the classical period thereby dragging it out of phase with the quantum mechanical results and damping the magnitude of the angular momentum transfer in the process.

Controlling the de-phasing therefore remains key to improving the results of the classical model. However, just like de-coherence in quantum systems, de-phasing is not something one can eliminate completely, reducing it should as such be the aim. A future study on the origin of de-phasing in such systems would be quite enlightening.

Chapter 5

Conclusion

The aim of this thesis was to study circular Rydberg states and to find parameters for which energy and angular momentum can be better transferred using these states. As a tribute to *correspondence principle*, that aims to find classical analogues of certain quantum mechanical phenomena, we started by studying angular momentum transfer through two interacting highly excited Alkali atoms by solving their coupled classical equations. The transfer was found to be resonant and oscillatory for some time before being damped by dephasing. This further establishes high-lying Bohr-like orbits as classical analogues of circular Rydberg states.

Quantum mechanical formulation of circular states and interaction between atoms in circular states was then studied. The circular state wavefunctions were found to, other than being non-symmetric, resemble $3D$ Harmonic oscillator wavefunctions with the most circular state corresponding to the ground state.

The dipole-dipole interaction between the atoms was then used to study energy and angular momentum transfer using circular states, with two atoms in the most circular states of a given quantum level n. The transfer for perfectly aligned internuclear and quantization axis case was found to be resonant and lasts for as long a time as the lifetime of the state without being damped, with transfer periods

in the lower μs range and scaling as n^{-3}.

The more realistic, slightly off-axis case, was also studied for different orientations and was found to be damped, resulting in loss of coherence in the transfer and subsequent angular momentum transfer to undesired lower states for angles $\alpha > 5°$. For $\alpha < 5°$ as much as 100% transfer is possible in $4\mu s$ which is less than the lifetime, $4.2\mu s$, of the $n = 10$ circular Rydberg state. Proper trapping of the atomic samples plays a central role here.

The findings of this study open up the possibility of using circular Rydberg states as better alternatives to the $|ns\rangle$ and $|np\rangle$ Rydberg states used so far in simulating energy transport mechanisms in light-harvesting systems using flexible and/or static Rydberg aggregates.

The use of flexible Rydberg aggregates, assemblies of Rydberg atoms confined to move in a given direction, or static aggregates that remain frozen and/or static over a given time scale, in circular states to perform transfer operations would be quite rewarding since the atomic motion that could manifest itself as noise in the system is now being put to use thus negating possible losses due to uncertainty in the atomic positions. This represents one of our future goals.

Also, finding pair circular states with comparable C_3 values that only transfer to each other could find application in the field of quantum information as data-bus.

We are convinced that, the possibility of having two circular states that only couple to each other, their longer lifetimes, coupled with the parameters and results of this study present circular states as better alternatives to use in energy and angular momentum transfer mechanisms.

Bibliography

[1] T. F. Gallagher, *Rydberg atoms*, vol. 3. Cambridge University Press, 2005.

[2] S. Chung and C. C. Lin, "Excitation of the electronic states of the nitrogen molecule by electron impact," *Physical Review A*, vol. 6, no. 3, p. 988, 1972.

[3] M. Haugh, T. Slanger, and K. Bayes, "Electronic excitation accompanying charge exchange," *The Journal of Chemical Physics*, vol. 44, no. 2, pp. 837–839, 1966.

[4] T. MAIMAN, "Stimulated optical radiation in ruby," *Nature*, vol. 187, no. 4736, pp. 493–494, 1960.

[5] T. Amthor, M. R. Lamour, C. Giese, and M. Weidemüller, "Modeling many-particle mechanical effects of an interacting rydberg gas," *Physical Review A*, vol. 76, no. 5, p. 054702, 2007.

[6] C. Ates, T. Pohl, T. Pattard, and J. Rost, "Antiblockade in rydberg excitation of an ultracold lattice gas," *Physical Review Letters*, vol. 98, no. 2, p. 23002, 2007.

[7] T. Amthor, C. Giese, C. S. Hofmann, and M. Weidemueller, "Evidence of antiblockade in an ultracold rydberg gas," *Physical Review Letters*, vol. 104, no. 1, 2010.

[8] M. Lukin, M. Fleischhauer, R. Cote, L. Duan, D. Jaksch, J. Cirac, and P. Zoller, "Dipole blockade and quantum information processing in mesoscopic atomic ensembles," *Physical Review Letters*, vol. 87, no. 3, p. 037901, 2001.

[9] E. Urban *et al.*, "Nature phys. 5, 110 (2009); a. gaetan et al," *Nature Phys*, vol. 5, p. 115, 2009.

[10] T. Wilk, A. Gaëtan, C. Evellin, J. Wolters, Y. Miroshnychenko, P. Grangier, and A. Browaeys, "Entanglement of two individual neutral atoms using rydberg blockade," *Physical Review Letters*, vol. 104, no. 1, p. 010502, 2010.

[11] M. Saffman, T. G. Walker, and K. Mølmer, "Quantum information with rydberg atoms," *Reviews of Modern Physics*, vol. 82, no. 3, p. 2313, 2010.

[12] R. Hulet and D. Kleppner, "Rydberg atoms in'circular'states," *Physical Review Letters*, vol. 51, pp. 1430–1433, 1983.

[13] T. Xia, X. Zhang, and M. Saffman, "Analysis of a controlled phase gate using circular rydberg states," *Physical Review A*, vol. 88, no. 6, p. 062337, 2013.

[14] J. Hare, A. Nussenzweig, C. Gabbanini, M. Weidemuller, P. Goy, M. Gross, and S. Haroche, "Toward a rydberg constant measurement on circular atoms," *IEEE transactions on instrumentation and measurement*, vol. 42, no. 2, pp. 331–334, 1993.

[15] R. Lutwak, J. Holley, P. P. Chang, S. Paine, D. Kleppner, and T. Ducas, "Circular states of atomic hydrogen," *Physical Review A*, vol. 56, no. 2, p. 1443, 1997.

[16] R. Hulet, E. Hilfer, and D. Kleppner, "Inhibited spontaneous emission by a rydberg atom," *Physical Review Letters*, vol. 55, pp. 2137–2140, 1985.

[17] M. Brune, E. Hagley, J. Dreyer, X. Maitre, A. Maali, C. Wunderlich, J. Raimond, and S. Haroche, "Observing the progressive decoherence of the meter in a quantum measurement," *Physical Review Letters*, vol. 77, no. 24, p. 4887, 1996.

[18] S. Gleyzes, S. Kuhr, C. Guerlin, J. Bernu, S. Deléglise, H. U. Busk, M. Brune, J. Raimond, and S. Haroche, "Quantum jumps of light recording the birth and death of a photon in a cavity.," *Nature*, vol. 446, no. 7133, p. 297, 2007.

[19] J. Hare, M. Gross, and P. Goy, "Circular atoms prepared by a new method of crossed electric and magnetic fields," *Physical Review Letters*, vol. 61, pp. 1938–1941, 1988.

[20] R. Brecha, G. Raithel, C. Wagner, and H. Walther, "Circular rydberg states with very large n," *Optics Communications*, vol. 102, pp. 257–264, 1993.

[21] D. Anderson, A. Schwarzkopf, R. Sapiro, and G. Raithel, "Production and trapping of cold circular rydberg atoms," *Physical Review A*, vol. 88, no. 3, 2013.

[22] W. Anderson, J. Veale, and T. Gallagher, "Resonant dipole-dipole energy transfer in a nearly frozen rydberg gas," *Physical Review Letters*, vol. 80, pp. 249–252, 1998.

[23] L. Wenhui, P. J. Tanner, and T. Gallagher, "Dipole-dipole excitation and ionization in an ultracold gas of rydberg atoms," *Physical Review Letters*, vol. 94, no. 17, 2005.

[24] S. Wüster, C. Ates, A. Eisfeld, and J. Rost, "Newton's cradle and entanglement transport in a flexible rydberg chain," *Physical Review Letters*, vol. 105, no. 5, 2010.

[25] N. Bohr, "I. on the constitution of atoms and molecules," *The London, Edinburgh, and Dublin Philosophical Magazine and Journal of Science*, vol. 26, no. 151, pp. 1–25, 1913.

[26] A. Sommerfeld, "On the theory of the balmer series*. presented at the meeting on 6 december 1915," *European Physical Journal H*, vol. 39, pp. 157–177, 2014.

[27] A. Sommerfeld, "The fine structure of hydrogen and hydrogen-like lines*. presented at the meeting on 8 january 1916," *European Physical Journal H*, vol. 39, pp. 179–204, 2014.

[28] A. Messiah, "Quantum mechanics, two volumes," 1999.

[29] M. Marinescu, H. Sadeghpour, and A. Dalgarno, "Dispersion coefficients for alkali-metal dimers," *Physical Review A*, vol. 49, no. 2, p. 982, 1994.

[30] J. Han, Y. Jamil, D. Norum, P. J. Tanner, and T. Gallagher, "Rb n f quantum defects from millimeter-wave spectroscopy of cold rb 85 rydberg atoms," *Physical Review A*, vol. 74, no. 5, p. 054502, 2006.

[31] W. Li, I. Mourachko, M. Noel, and T. Gallagher, "Millimeter-wave spectroscopy of cold rb rydberg atoms in a magneto-optical trap: Quantum defects of the ns, np, and nd series," *Physical Review A*, vol. 67, no. 5, p. 052502, 2003.

[32] T. Amthor, *Interaction-Induced Dynamics in Ultracold Rydberg Gases–Mechanical Effects and Coherent Processes*. PhD thesis, Ph. D. thesis, Fakultät für Mathematik und Physik, Albert-Ludwigs-Universität Freiburg, 2008.

[33] G. K. Campbell, "Atomic physics: When ultracold is not cold enough," *Nature*, vol. 480, no. 7378, pp. 463–465, 2011.

[34] H. Zoubi, A. Eisfeld, and S. Wüster, "Van-der-waals stabilized rydberg aggregates," *Phys. Rev. A*, vol. 89, no. arXiv: 1312.7319, p. 053426, 2013.

[35] A. U. Kowalczyk, *Manipulation and control of ultra-cold rubidium atoms*. PhD thesis, Open University, 2013.

[36] N. Henkel, "Rydberg-dressed bose-einstein condensates," 2013.

[37] K. M. Gheri, K. Ellinger, T. Pellizari, and P. Zoller, "Photon-wavepackets as flying quantum bits," *Fortschritte der Physik*, vol. 46, no. 4, pp. 401–416, 1998.

[38] Y. L. Lim, S. D. Barrett, A. Beige, P. Kok, and L. C. Kwek, "Repeat-until-success quantum computing using stationary and flying qubits," *Physical Review A*, vol. 73, no. 1, p. 012304, 2006.

[39] W. Yao, R. Liu, and L. Sham, "Theory of control of the spin-photon interface for quantum networks," *Physical Review Letters*, 2005.

[40] A. Ashkin, "Optical trapping and manipulation of neutral particles using lasers," *Proceedings of the National Academy of Sciences*, vol. 94, no. 10, pp. 4853–4860, 1997.

[41] H. J. Metcalf and P. Van der Straten, *Laser cooling and trapping*. Springer Science & Business Media, 2012.

[42] M. Weidemüller and C. Zimmermann, *Interactions in ultracold gases: from atoms to molecules*. John Wiley & Sons, 2011.

[43] E. Arimondo, W. D. Phillips, and F. Strumia, *Laser manipulation of atoms and ions*, vol. 118. Elsevier, 1993.

[44] F. Robicheaux, J. Hernández, T. Topçu, and L. Noordam, "Simulation of coherent interactions between rydberg atoms," *Physical Review A*, vol. 70, no. 4, p. 042703, 2004.

Appendix A

Dipole-dipole potential

From equation 3.13

$$V(\mathbf{R},\mathbf{a},\mathbf{b}) = \frac{1}{|\mathbf{R}|} - \frac{1}{|\mathbf{R}+\mathbf{b}|} - \frac{1}{|\mathbf{R}-\mathbf{a}|} + \frac{1}{|\mathbf{R}-(\mathbf{a}-\mathbf{b})|}. \tag{A.1}$$

Using binomial expansion

$$(1+x)^{-1/2} = 1 - \frac{x}{2} + \frac{3x^2}{8} + ... \tag{A.2}$$

$$\begin{aligned}\frac{1}{|\mathbf{R}+\mathbf{b}|} = \frac{1}{\sqrt{R^2+b^2+2\mathbf{R}.\mathbf{b}}} = \frac{1}{R}\left[1+\left(\frac{b^2}{R^2}+\frac{2\mathbf{R}.\mathbf{b}}{R^2}\right)\right]^{\frac{-1}{2}} \rightarrow \\ = \frac{1}{R}\left[1-\frac{1}{2}\left(\frac{b^2}{R^2}+\frac{2\mathbf{R}.\mathbf{b}}{R^2}\right)+\frac{3}{8}\left(\frac{b^2}{R^2}+\frac{2\mathbf{R}.\mathbf{b}}{R^2}\right)^2\right] \\ = \frac{1}{R}\left[1-\frac{1}{2}\left(\frac{b^2}{R^2}+\frac{2\mathbf{R}.\mathbf{b}}{R^2}\right)+\frac{3}{8}\left(\frac{b^4}{R^4}+\frac{4b^2\mathbf{R}.\mathbf{b}}{R^4}+4\frac{(\mathbf{R}.\mathbf{b})^2}{R^4}\right)\right]\end{aligned} \tag{A.3}$$

$$\begin{aligned}\frac{1}{|\mathbf{R}-\mathbf{a}|} = \frac{1}{\sqrt{R^2+a^2-2\mathbf{R}.\mathbf{a}}} = \frac{1}{R}\left[1+\left(\frac{a^2}{R^2}-\frac{2\mathbf{R}.\mathbf{a}}{R^2}\right)\right]^{\frac{-1}{2}} \rightarrow \\ = \frac{1}{R}\left[1-\frac{1}{2}\left(\frac{a^2}{R^2}-\frac{2\mathbf{R}.\mathbf{a}}{R^2}\right)+\frac{3}{8}\left(\frac{b^2}{R^2}-\frac{2\mathbf{R}.\mathbf{a}}{R^2}\right)^2\right] \\ = \frac{1}{R}\left[1-\frac{1}{2}\left(\frac{a^2}{R^2}-\frac{2\mathbf{R}.\mathbf{a}}{R^2}\right)+\frac{3}{8}\left(\frac{a^4}{R^4}-\frac{4a^2\mathbf{R}.\mathbf{a}}{R^4}+4\frac{(\mathbf{R}.\mathbf{a})^2}{R^4}\right)\right]\end{aligned} \tag{A.4}$$

and for

$$\frac{1}{|\mathbf{R}-(\mathbf{a}\text{-}\mathbf{b})|}=\frac{1}{\sqrt{1+\frac{a^2+b^2}{R^2}+\frac{\text{-}\mathbf{R}.\mathbf{a}+\mathbf{R}.\mathbf{b}-2\mathbf{a}.\mathbf{b}}{R^2}}}\rightarrow \tag{A.5}$$

$$=\frac{1}{R}\left[1-\frac{1}{2}\left(\frac{b^2+a^2}{R^2}+\frac{(\text{-}\mathbf{R}.\mathbf{a}+\mathbf{R}.\mathbf{b}-2\mathbf{a}.\mathbf{b})}{R^2}\right)+\frac{3}{8}\left(\frac{b^2+a^2}{R^2}+\frac{(\text{-}\mathbf{R}.\mathbf{a}+\mathbf{R}.\mathbf{b}-2\mathbf{a}.\mathbf{b})}{R^2}\right)^2\right],$$

by adding up all the terms one gets

$$V(\mathbf{R},\mathbf{a},\mathbf{b})=\frac{1}{R}\Bigg[1-\left[1-\frac{1}{2}\left(\frac{b^2}{R^2}+\frac{2\mathbf{R}.\mathbf{b}}{R^2}\right)+\frac{3}{8}\left(\frac{b^4}{R^4}+\frac{4b^2\mathbf{R}.\mathbf{b}}{R^4}+4\frac{(\mathbf{R}.\mathbf{b})^2}{R^4}\right)\right] \tag{A.6}$$

$$-\left[1-\frac{1}{2}\left(\frac{a^2}{R^2}-\frac{2\mathbf{R}.\mathbf{a}}{R^2}\right)+\frac{3}{8}\left(\frac{a^4}{R^4}-\frac{4a^2\mathbf{R}.\mathbf{a}}{R^4}+4\frac{(\mathbf{R}.\mathbf{a})^2}{R^4}\right)\right]$$

$$+\left[1-\frac{1}{2}\left(\frac{b^2+a^2}{R^2}+\frac{(\text{-}\mathbf{R}.\mathbf{a}+\mathbf{R}.\mathbf{b}-2\mathbf{a}.\mathbf{b})}{R^2}\right)+\frac{3}{8}\left(\frac{b^2+a^2}{R^2}+\frac{(\text{-}\mathbf{R}.\mathbf{a}+\mathbf{R}.\mathbf{b}-2\mathbf{a}.\mathbf{b})}{R^2}\right)^2\right]\Bigg],$$

and ignoring terms of order $\frac{a^2}{R^2}$, $\frac{b^2}{R^2}$ and higher, results in the dipole-dipole potential

$$V(\mathbf{R},\mathbf{a},\mathbf{b})=\frac{\mathbf{a}.\mathbf{b}}{R^3}-3\frac{(\mathbf{a}.\mathbf{R})(\mathbf{b}.\mathbf{R})}{R^5}. \tag{A.7}$$

Appendix B

Analytical circular wavefunctons and Clebsch-Gordan coefficients

Using equations 3.6 and 3.7

$$R_{nl}(r) = \sqrt{(\frac{2}{n})^3 \frac{(n-l-1)!}{2n(n+l)!}} \exp\Big(-\frac{r}{n}\Big) L_{n-l-1}^{2l+1}\Big(\frac{2r}{n}\Big)\Big(\frac{2r}{n}\Big)^l, \tag{B.1}$$

$$Y_m^l(\theta,\phi) = \sqrt{\frac{(2l+1)(l-m)!}{4\pi(l+m)!}} P_m^l\Big(\cos\theta\Big) \exp\Big(im\phi\Big), \tag{B.2}$$

for the circular states $(n, l = n-1, m = n-1)$ and $(n, l = n-2, m = n-2)$, we have

$$L_0^{(2n-1)}(\frac{2r}{n}) = 1 \tag{B.3}$$

$$L_1^{(2n-3)}(\frac{2r}{n}) = \left((2n-2) - \frac{2r}{n}\right) \tag{B.4}$$

$$R_{(n,n-1)}(r) = \sqrt{\Big(\frac{2}{n}\Big)^3 \frac{1}{2n(2n-1)!}}\Big(\frac{2r}{n}\Big)^{n-1}\Big[r^{n-1}\exp\Big(\frac{-r}{n}\Big)\Big] \tag{B.5}$$

$$R_{(n,n-1)}(r) = \sqrt{\Big(\frac{2}{n}\Big)^3 \frac{1}{2n(2n-2)!}}\Big(\frac{2r}{n}\Big)^{n-2}\Big[r^{n-2}\exp\Big(\frac{-r}{n}\Big)\Big]\Big[(2n-2) - \frac{2r}{n}\Big]. \tag{B.6}$$

And using equation 3.7, with $\cos\theta = x$

$$P_l^m(x) = \frac{(-1)^l}{2^l.l!}\Big(1-x^2\Big)^{\frac{m}{2}}\frac{d^{l+m}}{dx^{l+m}}\Big(x^2-1\Big)^l, \tag{B.7}$$

for $l = m$

$$P_l^l(cos\theta) = \frac{(-1)^l}{2^l.l!}\sin\theta(2l)!, \tag{B.8}$$

$$Y_l^l(\theta,\phi) = \frac{(-1)^l}{2^l.l!}\sqrt{\frac{2l+1}{4\pi}.(2l)!}\Big[\sin\theta.\exp(i\phi)\Big]^l, \tag{B.9}$$

by using $l = n-1$ and $l = n-2$ we get the expressions

$$Y_{n-1}^{n-1}(\theta,\phi) = \frac{(-1)^{n-1}}{2^{n-1}(n-1)!}\sqrt{\frac{(2n-2)!(2n-1)}{4\pi}}\Big(\sin\theta.\exp(i\phi)\Big)^{n-1}, \tag{B.10}$$

$$Y_{n-2}^{n-2}(\theta,\phi) = \frac{(-1)^{n-2}}{2^{n-2}(n-2)!}\sqrt{\frac{(2n-4)!(2n-3)}{4\pi}}\Big(\sin\theta.\exp(i\phi)\Big)^{n-2}. \tag{B.11}$$

To obtain the Clebsch-Gordan coefficients we make the transformation

$$|l,m\rangle = \sum_{m_1,m_2} C(l_1,m_1,l_2,m_2;l,m)|l_1,m_1,l_2,m_2\rangle, \tag{B.12}$$

with $m = -2,-1,0,1,2$, $l = 2$

$$\begin{aligned}
|2,-2\rangle &= |1,0,1,-1\rangle \\
|2,-1\rangle &= \frac{1}{\sqrt{2}}\Big(|1,-1,1,0\rangle + |1,0,1,-1\rangle\Big) \\
|2,0\rangle &= \frac{1}{\sqrt{6}}\Big(|1,-1,1,1\rangle + |1,1,1,-1\rangle + |1,0,1,0\rangle\Big) \\
|2,1\rangle &= \frac{1}{\sqrt{2}}\Big(|1,1,1,0\rangle + |1,0,1,1\rangle\Big) \\
|2,2\rangle &= |1,1,1,1\rangle,
\end{aligned} \tag{B.13}$$

for $\theta = 0$ and $\phi = 0$ only the $|2,0\rangle$ term survives, which in terms of spherical harmonics is

$$|2,0\rangle = \frac{1}{\sqrt{6}}\left(Y_{1,-1}^{(1)}Y_{1,1}^{(2)} + Y_{1,1}^{(1)}Y_{1,-1}^{(2)} + 2Y_{1,0}^{(1)}Y_{1,0}^{(2)}\right), \tag{B.14}$$

where the (1) and (2) indexes label the atoms.